N62 59654

Copy No. 7

N62 59654

RM No. L8C22

NACA RM No. L8C22

CASE FILE COPY

RESEARCH MEMORANDUM

SOME FLIGHT MEASUREMENTS OF PRESSURE-DISTRIBUTION AND BOUNDARY-LAYER CHARACTERISTICS IN THE PRESENCE OF SHOCK

By

John A. Zalovcik and Ernest P. Luke

Langley Aeronautical Laboratory
Langley Field, Va.

DOCUMENT ON LOAN FROM THE FILES OF
NATIONAL ADVISORY COMMITTEE FOR AERONAUTICS
LANGLEY AERONAUTICAL LABORATORY
LANGLEY FIELD, HAMPTON, VIRGINIA
RN TO THE ABOVE ADDRESS.
ESTS FOR PUBLICATIONS SHOULD BE ADDRESSED
LLOWS:
TIONAL ADVISORY COMMITTEE FOR AERONAUTICS
12 H STREET, N. W.
SHINGTON 25, D. C.

CLASSIFICATION CANCELLED

CLASSIFIED DOCUMENT

This document contains classified information affecting the National Defense of the United States within the meaning of the Espionage Act, USC 50:31 and 32. Its transmission or the revelation of its contents in any manner to an unauthorized person is prohibited by law. Information so classified may be imparted only to persons in the military and naval services of the United States, appropriate civilian officers and employees of the Federal Government who have a legitimate interest therein, and to United States citizens of known loyalty and discretion who of necessity must be informed thereof.

NATIONAL ADVISORY COMMITTEE FOR AERONAUTICS

WASHINGTON

July 23, 1948

RESTRICTED

NACA LIBRARY
LANGLEY MEMORIAL AERONAUTICAL
LABORATORY
Langley Field, Va.

NATIONAL ADVISORY COMMITTEE FOR AERONAUTICS

RESEARCH MEMORANDUM

SOME FLIGHT MEASUREMENTS OF PRESSURE-DISTRIBUTION AND BOUNDARY-LAYER CHARACTERISTICS IN THE PRESENCE OF SHOCK

By John A. Zalovcik and Ernest P. Luke

SUMMARY

Some pressure-distribution and boundary-layer measurements were made in flight in the presence of shock on two modifications of the local contour of the wings of a high-speed airplane. One contour was designed to have maximum curvature at 32 and 56 percent chord on the upper surface and the other to have maximum curvature at 36 percent chord on the upper surface. The contours had practically the same critical Mach numbers (0.63 at a lift coefficient of 0.18). On the contour with the single curvature peak, shock formed immediately behind the peak curvature and moved downstream with increasing Mach number. On the other contour, shock first formed behind the first curvature peak and, as it moved downstream with increasing Mach number, a second shock appeared just behind the second curvature peak. At Mach numbers greater than 0.723 the first shock coalesced with the second downstream of the second curvature peak. Neither of the two shocks nor the combined shock was so intense as that on the contour with the single peak curvature. As a result, the effects of shock on the boundary layer, which was turbulent in the region of mixed flow on both contours, were more severe on the contour with the single curvature peak at least up to a flight Mach number of 0.731. On both contours the displacement thickness and the shape parameter (ratio of displacement thickness to momentum thickness) increased rapidly through shock. Downstream of shock the displacement thickness increased at a slower rate but the shape parameter decreased. The displacement thickness increased as much as 350 percent through shock on the contour with the single peak curvature. At the same time the shape parameter increased to about 4.0 behind shock but decreased to 1.9 farther downstream. (Values of the shape parameter of 1.8 to 2.6 are usually associated with separation or imminent separation at low speeds.) Surface tuft observations indicated separation of the turbulent boundary layer behind shock with reattachment downstream. No flow separation was observed from tuft surveys on the contour with the double peak curvature at least up to a flight Mach number of 0.731.

INTRODUCTION

In a recent study of airfoil contours for the wing-flow method of obtaining data at transonic speeds some pressure-distribution measurements and boundary-layer surveys were made in the presence of shock on two modifications of the local contour of the wings of a high-speed airplane. Because of the current interest in the interaction of shock and boundary layer, these measurements were extended somewhat beyond those planned for the original investigation.

The data presented are confined to flow with a turbulent boundary layer ahead of shock for Reynolds numbers, based on momentum thickness, up to 10,000. A very detailed wind-tunnel investigation of the interaction of shock with both laminar and turbulent boundary layers was reported in reference 1 by Ackeret, Feldmann, and Rott. The Reynolds number of the turbulent boundary layer investigated in reference 1 ranged from 1159 to 2315.

SYMBOLS

x	distance along chord from leading edge
y	distance above surface, or above chord line
c	wing section chord (74.5 in.)
r	local radius of curvature
M	Mach number
C_L	airplane lift coefficient
ρ	density
u	velocity
p	static pressure
p_t	total pressure
q	dynamic pressure $\left(\frac{1}{2}\rho u^2\right)$
δ^*	displacement thickness $\left(\int_0^\delta \left(1 - \frac{\rho u}{\rho_\delta u_\delta}\right) dy\right)$

θ momentum thickness $\left(\int_0^\delta \frac{\rho u}{\rho_\delta u_\delta}\left(1 - \frac{u}{u_\delta}\right) dy\right)$

δ boundary-layer thickness

H shape parameter (δ^*/θ)

R_e boundary-layer Reynolds number $(u_\delta \theta/\nu_\delta)$

ν kinematic viscosity

σ Prandtl number

T temperature, °R

Subscripts:

o free stream

δ edge of boundary layer

w wing surface

s shock

cr critical

u upper

l lower

APPARATUS AND TESTS

The two wing contours investigated were modifications of the wings of a P-51D airplane. The modification consisted of the addition of a metal bump to the upper surface between 10 and 75 percent chord and between 45 and 65 percent semispan. Except in the region where the bump faired into the wing surface, the bump had a thickness of at least 0.3 inch. This surface may therefore be considered as practically rigid. A sketch of the airfoil contours, referred to as contours A and B, is shown in figure 1 and the ordinates are given in table I.

Static-pressure measurements were made along the upper surface of both contours with 22 flush orifices located between 17 and 63 percent chord. Total-pressure measurements in the boundary layer

were made with racks of 8 or 11 total-pressure tubes. Static pressure in the boundary layer was measured only at the surface by means of an orifice at the same chordwise position as the boundary-layer rack but removed spanwise from it by 2 inches. All the pressures were recorded photographically with instruments using pressure diaphragms. The flow conditions in the boundary layer were also observed in some of the tests by means of tufts (wool yarn) attached to the upper surface of each contour from about 45 percent chord to the trailing edge. The behavior of the tufts was photographically recorded.

The tests were made in high-speed dives, from an altitude of 28,000 feet to about 21,000 feet, in which airplane Mach numbers from 0.53 to 0.75 were attained and during which the measurements were continuously recorded. For the boundary-layer surveys on contour A, the racks were located at 41.9 and 52.0 percent chord, as shown in figure 2, and the measurements were made simultaneously at these stations. Measurements were also made with a rack located only at 62.5 percent chord. On contour B, one rack was used on the surface per test (fig. 3) and the tests were repeated for rack positions at 45.6, 49.6, 54.4, and 62.3 percent chord.

RESULTS AND DISCUSSION

Pressure distribution.- Some distributions of local Mach number outside the boundary layer (M_δ) along the chord are presented in figures 4 and 5 for contours A and B, respectively. The local curvature $\frac{1}{r/c}$ as determined from measurements made with a curvature gage, is also plotted in each of figures 4 and 5. The design curvature is shown for comparison.

The distribution of M_δ for contour A, at subcritical speeds, indicated two positions of minimum pressure, one corresponding to maximum curvature at 32 percent chord and the other to maximum curvature at 56 percent chord. The curvature at 32 percent chord was greater than that at 56 percent chord. Local velocity of sound was first attained at the forward position of maximum curvature at an airplane Mach number of 0.635. At higher Mach numbers shock formed behind the forward position of maximum curvature and, as it moved downstream with increasing Mach number in the dive, shock was followed by an expansion to local supersonic flow and a second shock immediately behind the rear position of maximum curvature. In approaching the second position of minimum pressure the indicated compression shock decreased in magnitude. At free-stream Mach numbers greater than 0.723, the forward shock moved downstream of the rear position of maximum curvature, joined the rear shock, and thereby formed a single shock. Although the rearward movement of shock resulted principally from the increasing Mach number, there

was some effect from the decreasing lift coefficient which accompanied it during the dive. In the pull-out condition (high Mach number and increasing lift coefficient) shock moved upstream.

The distribution of M_δ on contour B at subcritical speeds indicated minimum pressure at the maximum curvature at 36 percent chord. At speeds greater than critical ($M_o = 0.632$) shock occurred behind the position of maximum curvature and moved downstream with increasing Mach number in the dive. In the pull-out condition (high Mach numbers and increasing lift coefficient) shock moved upstream and was followed by boundary-layer separation, as is indicated by the large values of M_δ behind shock. For corresponding flight conditions, the compression shock on this contour appeared to be more intense than that on contour A.

Boundary-layer surveys.- For the conditions investigated, the boundary layer was turbulent in the region of the surveys on both contours A and B. Some typical distributions of Mach number through the turbulent boundary layer are presented in figures 6 to 8 for contour A and in figures 9 to 12 for contour B. The variation with flight Mach number M_o of displacement thickness δ^*/c, momentum thickness θ/c, Mach number M_δ, and airplane lift coefficient C_L as obtained in the high-speed dives and pull-outs is shown in figures 13 and 14. A summary of the boundary-layer results is presented in figure 15 as a plot of the variation with flight Mach number M_o of δ^*/c, θ/c, δ/c, H, R_θ, C_L, and M_δ for both contours. Although θ/c, δ^*/c, and δ/c are presented as variations with flight Mach number M_o, these variations are also affected by lift coefficient principally as it affects the pressure distribution and possibly as it affects the position of transition. The value of δ was determined by plotting values of M/M_δ near the edge of the boundary layer against y on log-log paper, fairing the points with a straight line, and then extrapolating the straight line to $\frac{M}{M_\delta} = 1.0$. The evaluation of M, δ^*, and θ from the total- and static-pressure measurements is discussed in the appendix.

In two successive runs during the tests of contour A, the distribution of Mach number in the boundary layer, and consequently δ^* and θ, agreed for the survey rack at 41.9 percent chord but showed considerable differences for the rack at 52 percent chord. The differences for the rear position may be attributable to some form of interference of the forward rack on the flow at the rear rack; however, the local static pressure or M_δ did not reflect this interference.

On contour A the increase in displacement thickness through shock at 41.9 percent chord was about 62 percent. The value of R_θ ahead of shock was 5000. The shape parameter H immediately behind shock was in the range of values usually associated with separation, or imminent separation at low speeds (reference 2). At 10.1 and 20.6 percent chord

downstream of this shock the boundary layer was appreciably thicker, but the value of H had decreased to values somewhat smaller than those ahead of shock. The boundary-layer thickness δ/c showed practically no variation through shock. With shock occurring at 52 percent chord, the increase in displacement thickness through shock was in the range of 30 to 50 percent. The value of R_θ ahead of shock was 6000 to 8000. The smaller relative increase in displacement thickness through shock at 52 percent chord was probably associated with the fact that the compression in the boundary layer at 52 percent chord due to shock (as indicated by the magnitude of the abrupt change in M_δ in figs. 4 and 15) was about one-half the magnitude of the compression at 41.9 percent chord. The increase in the value of H through shock was small and was followed by a slight decrease at least up to 62.5 percent chord. The variation of boundary-layer thickness δ/c through shock, however, was considerable. For the test with the rack at 62.5 percent chord, the most rearward position of shock was at about 57.5 percent chord. For this condition, $M_o = 0.731$ and $C_L = 0.125$, the value of R_θ ahead of shock was estimated to be about 10,000. The increase in displacement thickness from ahead of shock (where thickness was estimated) to 5 percent chord downstream of shock (or 57.5 to 62.5 percent chord) was of the order of 300 percent. The value of H increased from about 1.9 to 2.8. Flow surveys made with surface tufts during this test indicated that the flow was smooth up to about 70 percent chord. Downstream of this position there was some unsteadiness in the flow (evident as slight tuft oscillations) such as is usually associated with thick boundary layers but no separation of the flow even though a value of H as high as 3.2 at 62.5 percent chord was attained in the pull-out. No lateral flow or cross flow was apparent from the tuft surveys.

On contour B the displacement thickness increased about 68 percent through shock at 45.6 percent chord and 120 percent at 49.6 percent chord. The boundary-layer thickness δ/c, however, showed no appreciable variation for either of these chordwise positions. The value of R_e ahead of shock for these conditions was 6400 and 7000 for 45.6 and 49.6 percent chord, respectively. With shock occurring somewhat ahead of 54.4 percent chord, the displacement thickness increased about 350 percent between 49.6 and 54.4 percent chord and then decreased about 30 percent between 54.4 and 62.3 percent chord. The Reynolds number ahead of shock for this condition was about 7000. The shape parameter H increased rapidly through shock and attained values at least as high as 4.0. Downstream of shock the value of H decreased. The values of H usually associated with separation or imminent separation at low speeds range from 1.8 to 2.6 (reference 2). The values of H in the vicinity of shock are summarized in the following table:

M_o	Shock immediately ahead of chordwise position, x/c	H			
		x/c			
		0.456	0.496	0.544	0.623
0.678	0.456	2.05	2.23	1.90	1.66
.688	.496	1.78	2.69	2.10	1.67
.713	.544	1.82	1.88	4.00	1.90

An attempt was made in figure 16 to correlate the chordwise distribution of local Mach number M_δ, the shape parameter H, and the behavior of the tufts. The behavior of the tufts and the values of H are indicated for each Mach number distribution curve. For conditions where the boundary-layer surveys showed the boundary layer to be definitely detached from the surface, the shape parameter was not evaluated but is indicated in figure 16 by a symbol d. In the region of shock, the tufts, in general, were observed to be oscillating and raised above the surface (at an appreciable angle in some cases). Downstream of this region the tufts were either lying upstream or flipping back and forth in the chordwise direction. Such a behavior of tufts at low speeds is usually associated with separated flow. Still farther downstream the tufts were lying downstream but oscillating laterally. The chordwise extent of local separation (tufts lying or flipping forward) increased as the flight Mach number was increased and also as shock moved forward with increasing lift coefficient. Although no specific values of H can be assigned to the tuft behavior noted, the tuft and boundary-layer surveys are in agreement in indicating separation with reattachment. In the region of local separation the distribution of M_δ (fig. 16) indicated a pressure recovery at least up to 62.3 percent chord or the most rearward position for the pressure-distribution measurements. At higher flight Mach numbers separation may be more severe since the local Mach number distribution in figure 5 (M_o = 0.739, 0.752 and C_L = 0.15, 0.16, respectively) indicated practically no pressure recovery beyond shock and up to at least 62.3 percent chord.

Effects on test airplane.- Although contours A and B had practically the same critical Mach number and differed by no more than 0.34 percent chord in thickness at any chordwise station, the pressure-distribution and boundary-layer characteristics were more favorable at high speeds on contour A than on contour B. In the high-speed dives and pull-outs, boundary-layer separation was indicated on contour B but not on contour A. Furthermore, the upper surface of contour A appeared to produce more lift in the pull-outs than the upper surface of contour B. These differences in flow characteristics acting on a small portion of the span were sufficient to cause an

unusual behavior of the test airplane. In the tests with contour A on the right wing and contour B on the left wing, the pilot reported that the airplane had to be trimmed to counteract left roll at a Mach number of about 0.73. This rolling tendency increased so much during the pull-out that in subsequent tests the flight Mach numbers in the dive were limited to lower values in order to retain sufficient lateral control during the pull-out. The maximum normal acceleration attainable in the pull-out was also lower and the buffeting more severe than for the normal airplane.

CONCLUDING REMARKS

Some pressure-distribution and boundary-layer measurements were made in the presence of shock on two local contour modifications of the wings of a P-51D airplane. One contour was designed to have maximum curvature at 32 and 56 percent chord of the upper surface and the other to have maximum curvature at 36 percent chord on the upper surface. The contours had about the same critical Mach number (0.63 at a lift coefficient of 0.18). On the contour with the single curvature peak, shock formed immediately behind the peak curvature and moved downstream with increasing Mach number. On the other contour, shock first formed behind the first curvature peak and, as it moved downstream with increasing Mach number, a second shock appeared just behind the second curvature peak. At Mach numbers greater than 0.723 the first shock coalesced with the second downstream of the second curvature peak. Neither of the two shocks nor the combined shock was so intense as that on the contour with the single peak curvature. As a result, the effects of shock on the boundary layer, which was turbulent in the region of mixed flow on both contours, were more severe on the contour with the single curvature peak at least up to a flight Mach number of 0.731. On both contours the displacement thickness and the shape parameter (ratio of displacement thickness to momentum thickness) increased rapidly through shock. Downstream of shock the displacement thickness increased at a slower rate but the shape parameter decreased. The displacement thickness increased as much as 350 percent through shock on the contour with the single peak curvature. At the same time the shape parameter increased to about 4.0 behind shock but decreased to 1.9 farther downstream. (Values of the shape parameter of 1.8 to 2.6 are usually associated with separation or imminent separation at low speeds.) Surface tuft observations indicated separation of the turbulent boundary layer behind shock with reattachment downstream. No flow separation was observed from tuft surveys on the contour with the double peak curvature at least up to a flight Mach number of 0.731.

Langley Aeronautical Laboratory
National Advisory Committee for Aeronautics
Langley Field, Va.

APPENDIX

Evaluation of M.- The value of M_δ was determined from static-pressure measurements in subsonic and supersonic flow by the use of Bernoulli's equation for compressible flow

$$\frac{p_{t_o}}{p} = \left(1 + \frac{\gamma - 1}{2} M_\delta^2\right)^{\frac{\gamma}{\gamma-1}}$$

where p_{t_o} is the free-stream total pressure measured by a pitot tube mounted on a boom ahead of the airplane wing. In the subsonic flow behind shock on the wing the use of the free-stream value of total pressure was justified by the boundary-layer measurements which showed that the total pressure immediately outside the boundary layer was within 1/2 percent (including experimental error) of free-stream total pressure. A normal shock extending into the boundary layer would have given a loss in total pressure of as much as 3 percent of free-stream total pressure in some cases.

The Mach number M in the boundary layer was determined from the total-pressure measurements by the use of Bernoulli's equation when $\frac{p_t}{p} \leqq 1.893$ (subsonic flow)

$$\frac{p_t}{p} = \left(1 + \frac{\gamma - 1}{2} M^2\right)^{\frac{\gamma}{\gamma-1}}$$

and the following expression (reference 3) when $\frac{p_t}{p} \geqq 1.893$ (supersonic flow)

$$\frac{p_t}{p} = \frac{(\gamma + 1)}{2} M^2 \left[\frac{(\gamma + 1)^2 M^2}{4\gamma M^2 - 2(\gamma - 1)}\right]^{\frac{1}{\gamma-1}}$$

In the boundary-layer measurements the static pressure was measured only at the surface. Since the static-pressure variation across the

boundary layer is of second order under ordinary pressure gradients and is also small in the presence of shock (see fig. 18 of reference 1), it was neglected in the computation of Mach number.

Evaluation of δ^* and θ.- The displacement thickness δ^* and momentum thickness θ are defined by the following equations:

$$\delta^* = \int_0^\delta \left(1 - \frac{\rho u}{\rho_\delta u_\delta}\right) dy$$

and

$$\theta = \int_0^\delta \frac{\rho u}{\rho_\delta u_\delta} \left(1 - \frac{u}{u_\delta}\right) dy$$

where

$$\frac{u}{u_\delta} = \frac{M}{M_\delta} \sqrt{\frac{T}{T_\delta}}$$

$$\frac{\rho u}{\rho_\delta u_\delta} = \frac{p}{p_\delta} \frac{T_\delta}{T} \frac{M}{M_\delta} \sqrt{\frac{T}{T_\delta}}$$

$$= \frac{M}{M_\delta} \sqrt{\frac{T_\delta}{T}}$$

and p/p_δ is assumed to be 1.0.

The temperature decrease from the wing surface to the edge of the boundary layer is shown in reference 4 to be:

$$T_w - T_\delta = \frac{\gamma - 1}{2} M_\delta{}^2 T_\delta \sigma^n$$

where

$$\sigma = 0.744 \quad \text{for} \quad T_\delta = 400$$

$$n = \frac{1}{3} \quad \text{for turbulent flow}$$

Therefore

$$\frac{T_w}{T_\delta} = 1 + 0.18{M_\delta}^2$$

If the distribution of the temperature difference between the surface and any point in the boundary layer is assumed to be similar to the Mach number distribution in the boundary layer, then:

$$\frac{T_w - T}{T_w - T_\delta} = \frac{M}{M_\delta}$$

or

$$\frac{T}{T_\delta} = 1 + \left(\frac{T_w}{T_\delta} - 1\right)\left(1 - \frac{M}{M_\delta}\right)$$

$$= 1 + 0.18{M_\delta}^2\left(1 - \frac{M}{M_\delta}\right)$$

REFERENCES

1. Ackeret, J., Feldmann, F., and Rott, N.: Investigations of Commpression Shocks and Boundary Layers in Gases Moving at High Speed. NACA TM No. 1113, 1947.

2. von Doenhoff, Albert E., and Tetervin, Neal: Determination of General Relations for the Behavior of Turbulent Boundary Layers. NACA ACR No. 3G13, 1943.

3. Taylor, G. I., and Maccoll, J. W.: The Mechanics of Compressible Fluids. Two-Dimensional Flow at Supersonic Speeds, Vol. III of Aerodynamic Theory, div. H, ch. IV, secs. 2 and 3, W. F. Durand, ed., Julius Springer (Berlin), 1935, pp. 236-242.

4. Squire, H. B.: Heat Transfer Calculation for Aerofoils. R. & M. No. 1986, British A.R.C., 1946.

TABLE I.- ORDINATES OF CONTOURS A AND B

FROM AN ARBITRARY CHORD LINE

x/c	y_l/c (both contours)	y_u/c	
		Contour A	Contour B
0	0	0	0
.125	.0167	.0185	.0185
.025	.0227	.0262	.0262
.050	.0302	.0374	.0374
.075	.0358	.0452	.0452
.10	.0403	.0519	.0519
.15	.0468	.0645	.0645
.20	.0517	.0752	.0752
.25	.0553	.0845	.0845
.30	.0578	.0911	.0920
.35	----------	.0939	.0956
.40	.0592	.0943	.0963
.45	----------	.0934	.0947
.50	.0559	.0914	.0900
.55	----------	.0873	.0839
.60	.0458	.0806	.0772
.65	----------	.0709	.0683
.70	.0312	.0584	.0575
.75	----------	.0450	.0450
.80	.0173	.0353	.0353
.90	.0054	.0145	.0145
.95	.0020	.0060	.0060
1.00	0	0	0

NACA

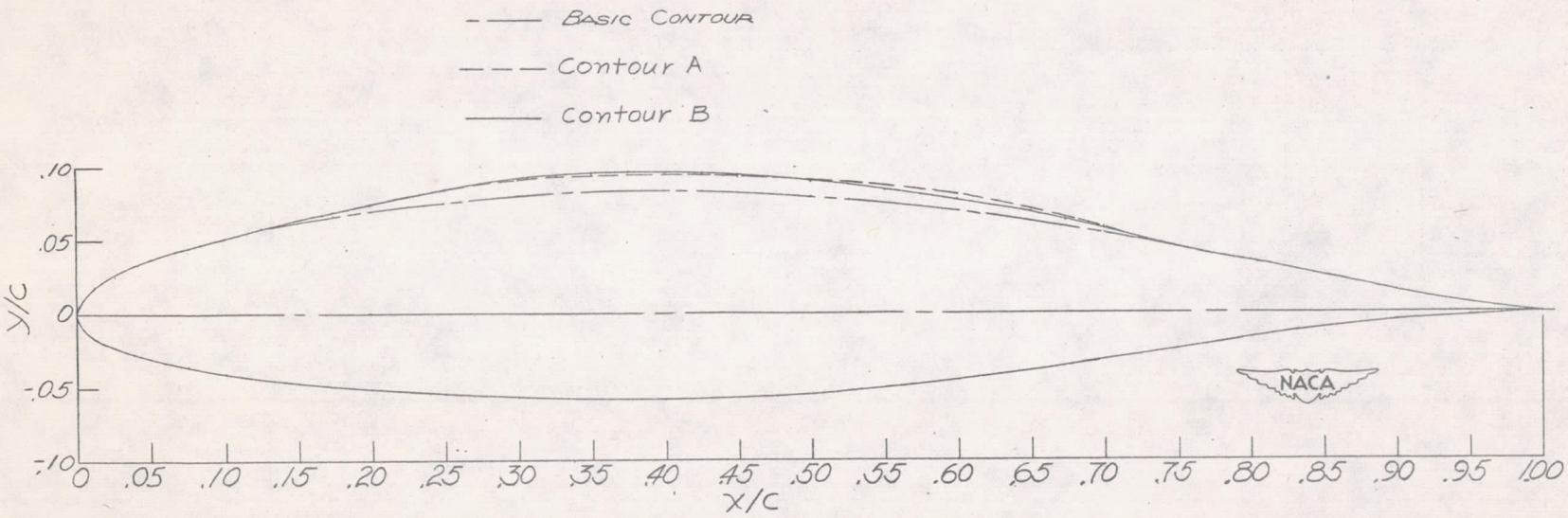

Figure 1.- Sketch of section of basic contour, contour A, and contour B.

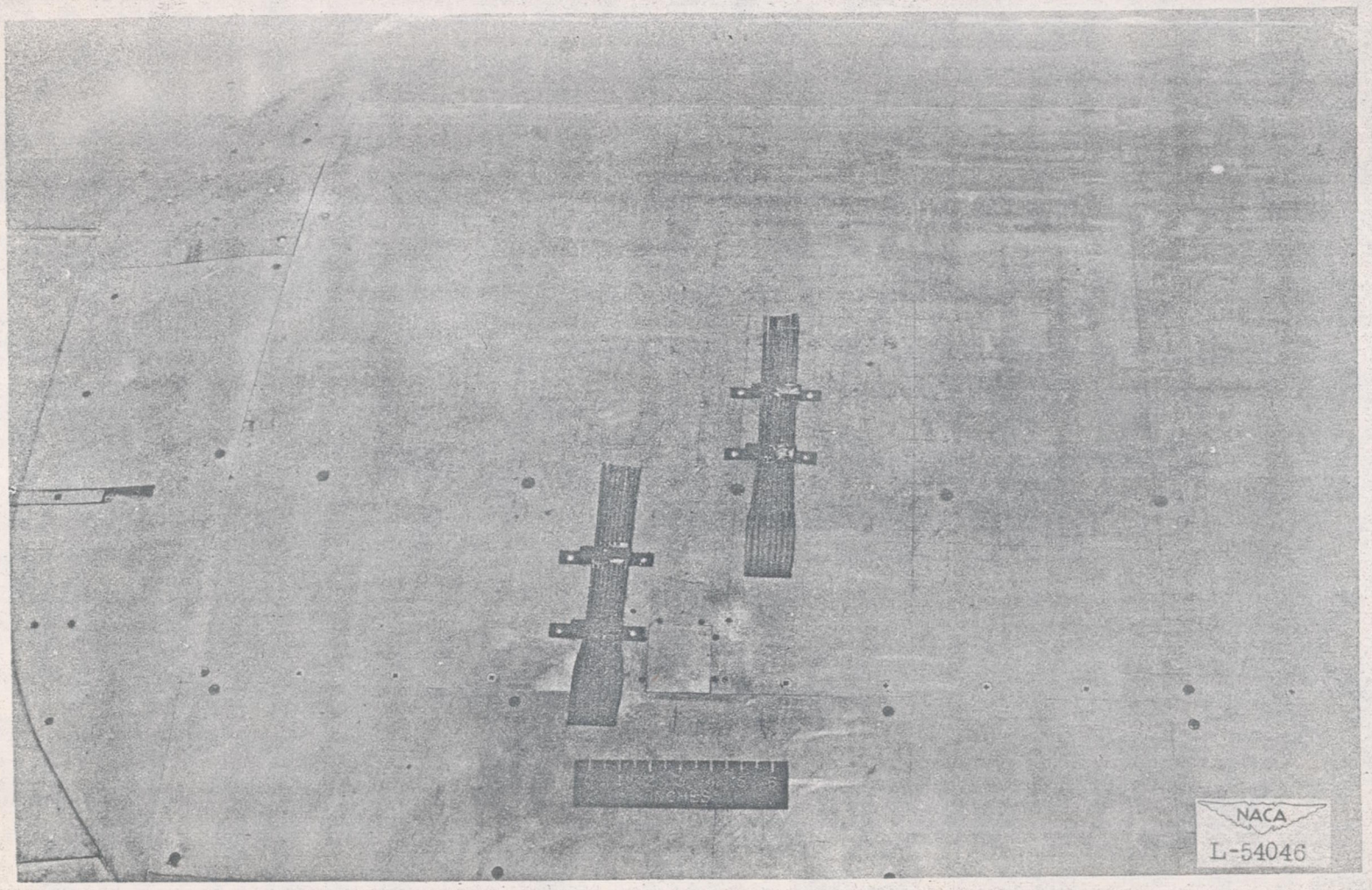

(a) Top view.

Figure 2.- Arrangement of boundary-layer racks at 41.9 and 52.0 percent chord on Contour A.

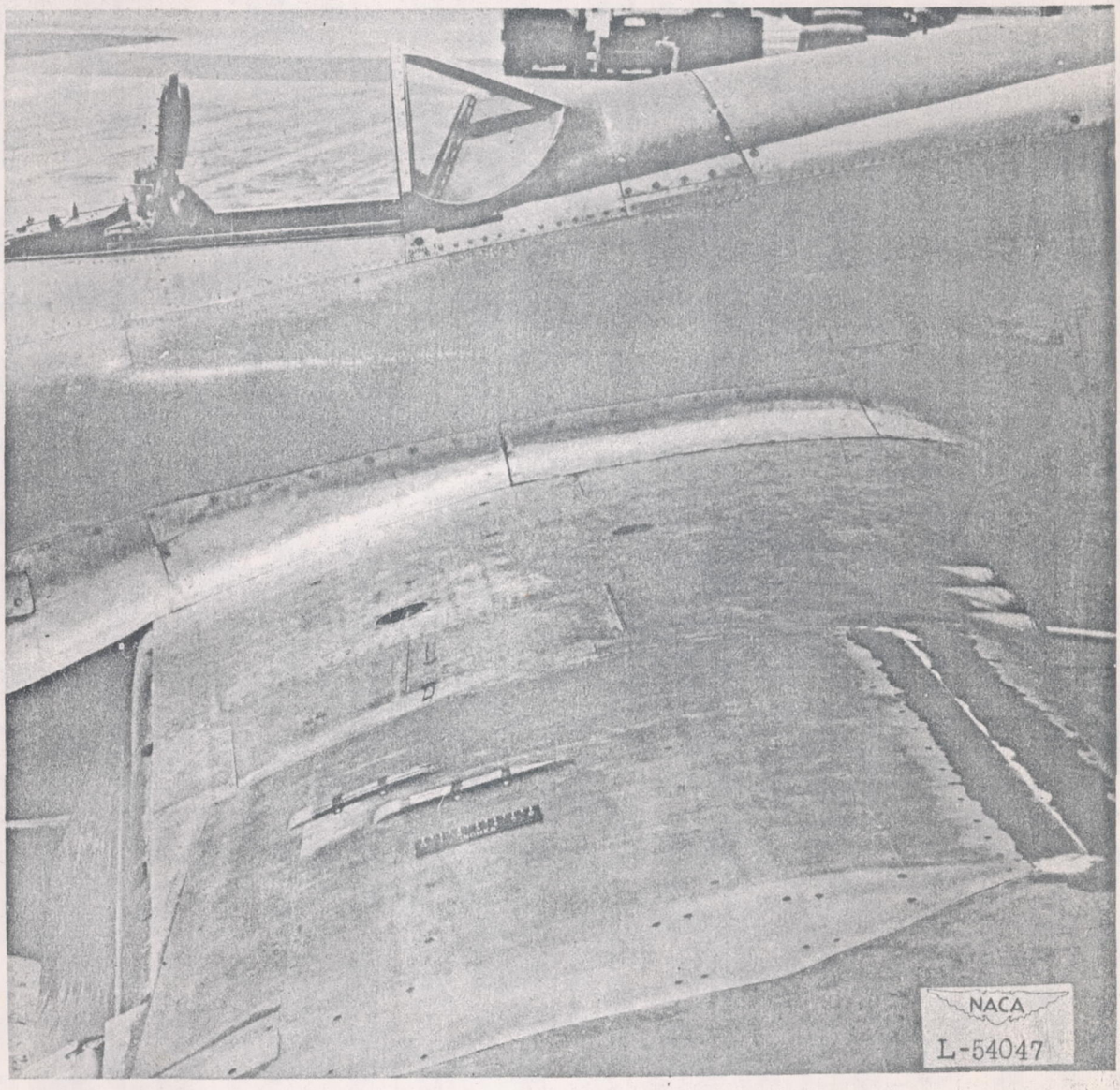

(b) Side view.

Figure 2.- Concluded.

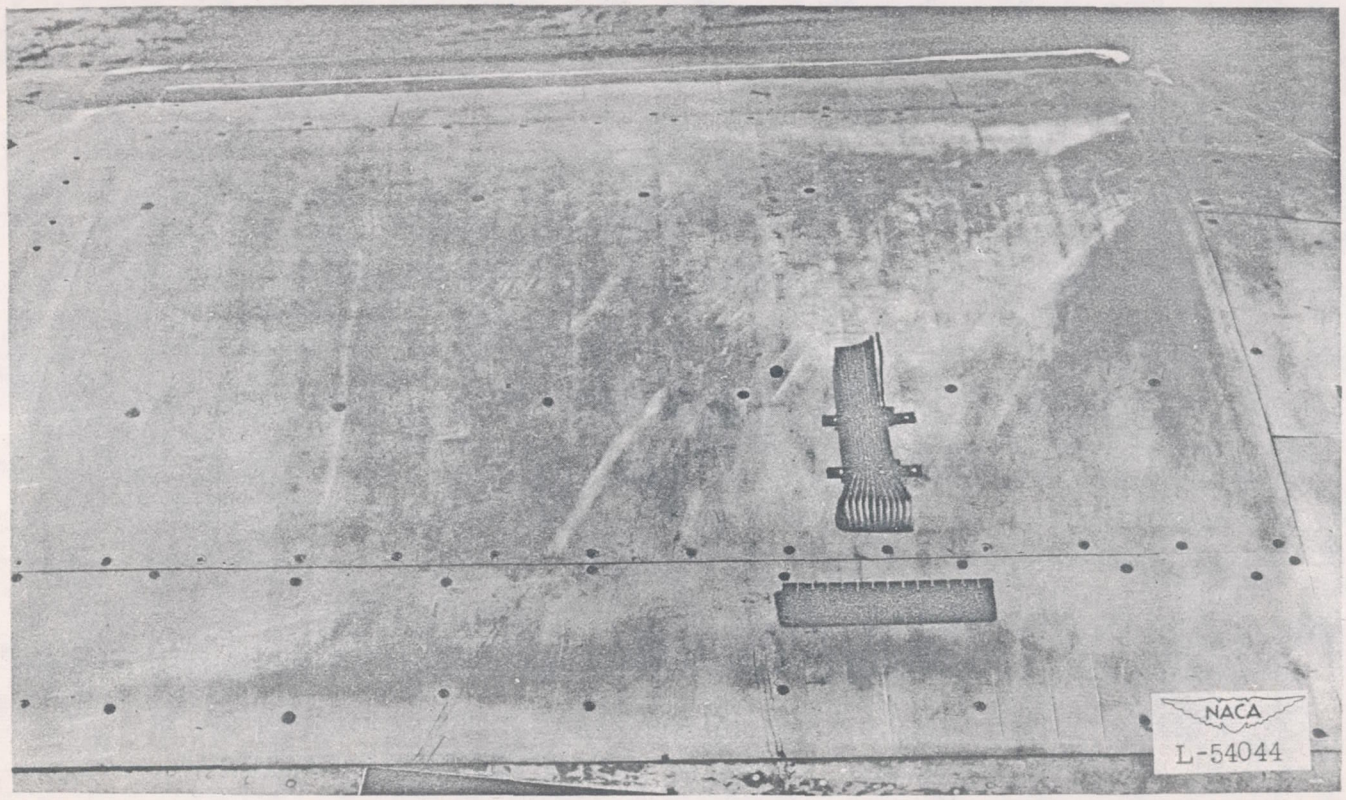

Figure 3.- Boundary-layer rack at 49.6 percent chord on Contour B.

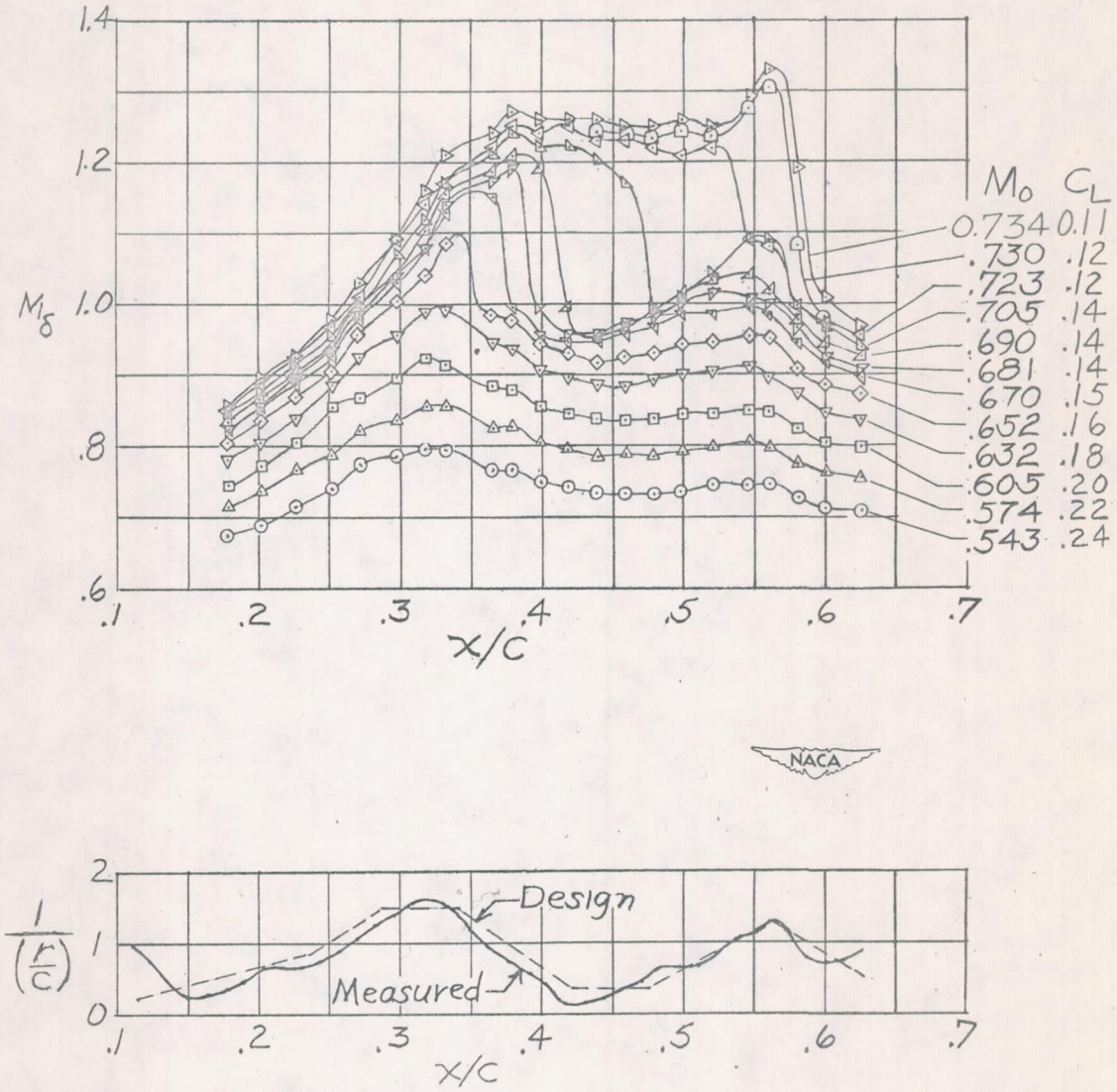

Figure 4.- Distribution of M_δ, for various values of M_o and C_L, along upper surface of contour A. Local curvature of the contour is also shown.

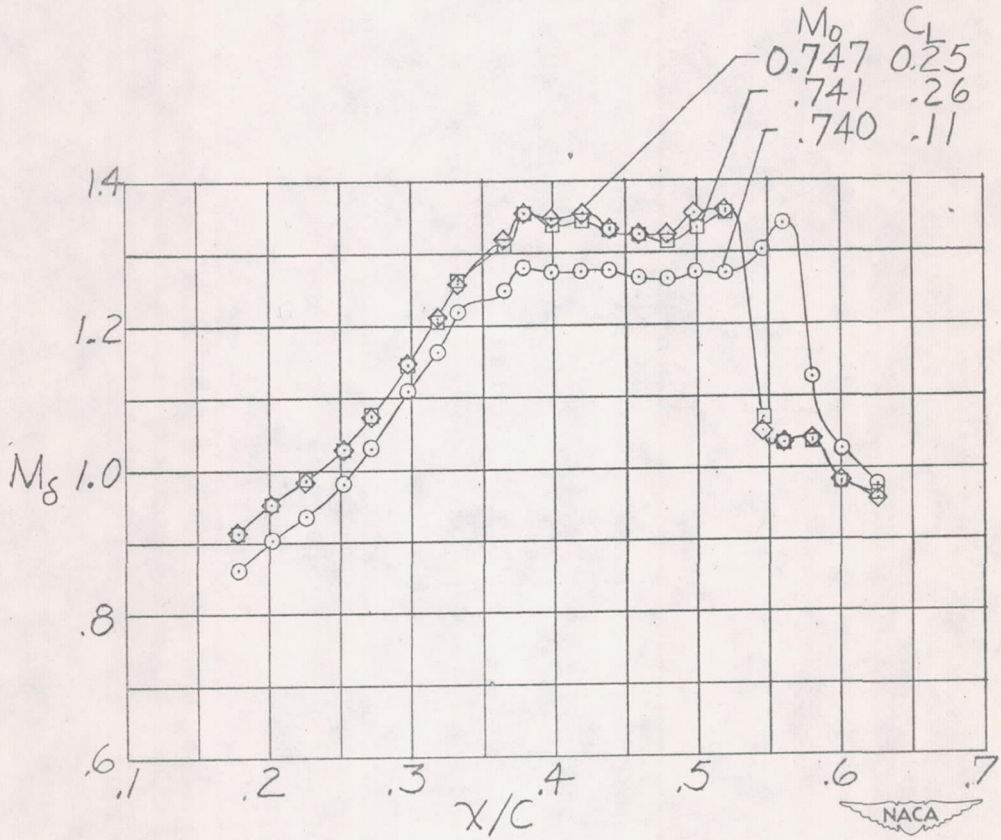

Figure 4.- Concluded.

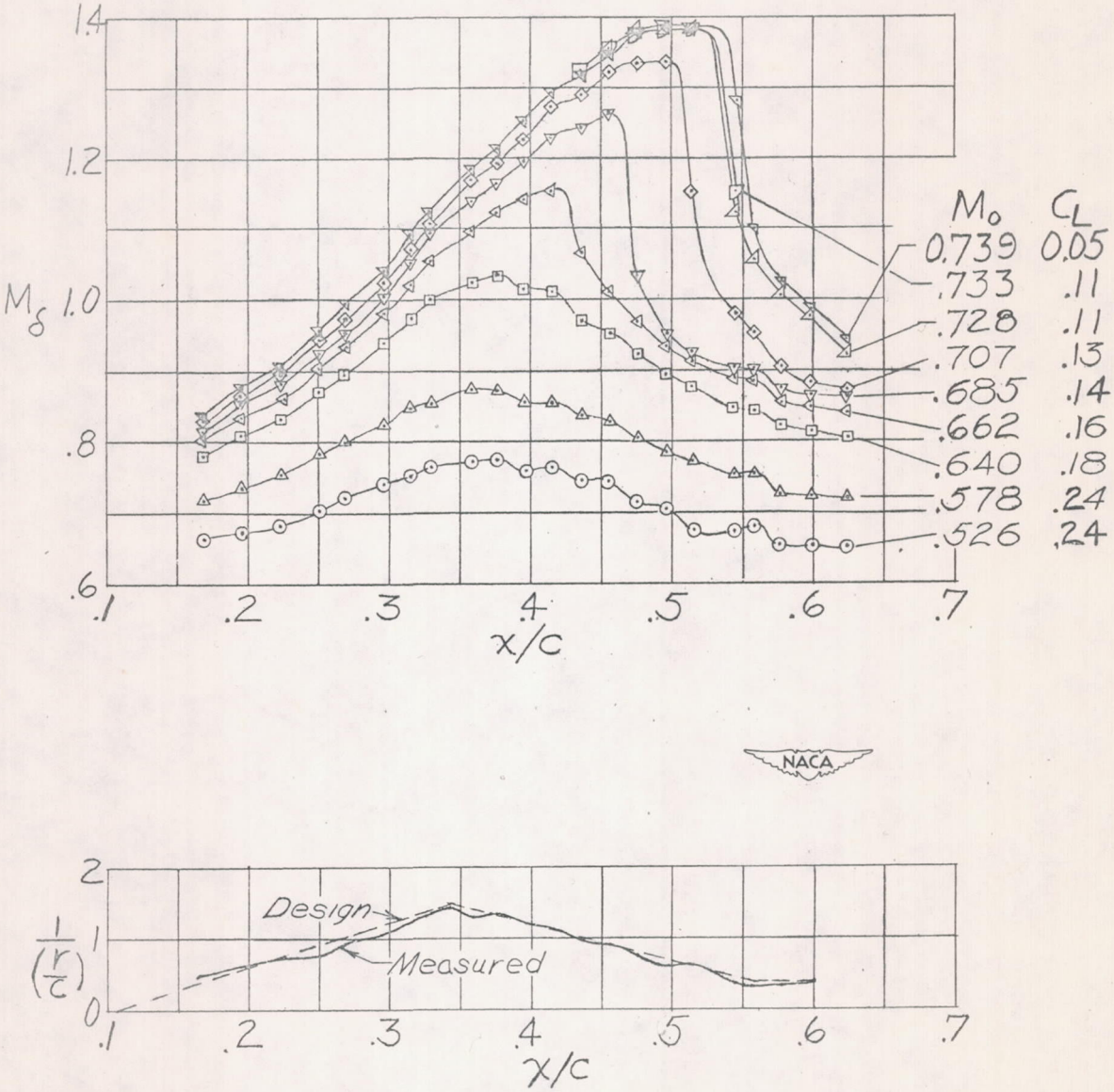

Figure 5.- Distribution of M_δ, for various values of M_o and C_L, along upper surface of contour B. Local curvature of the contour is also shown.

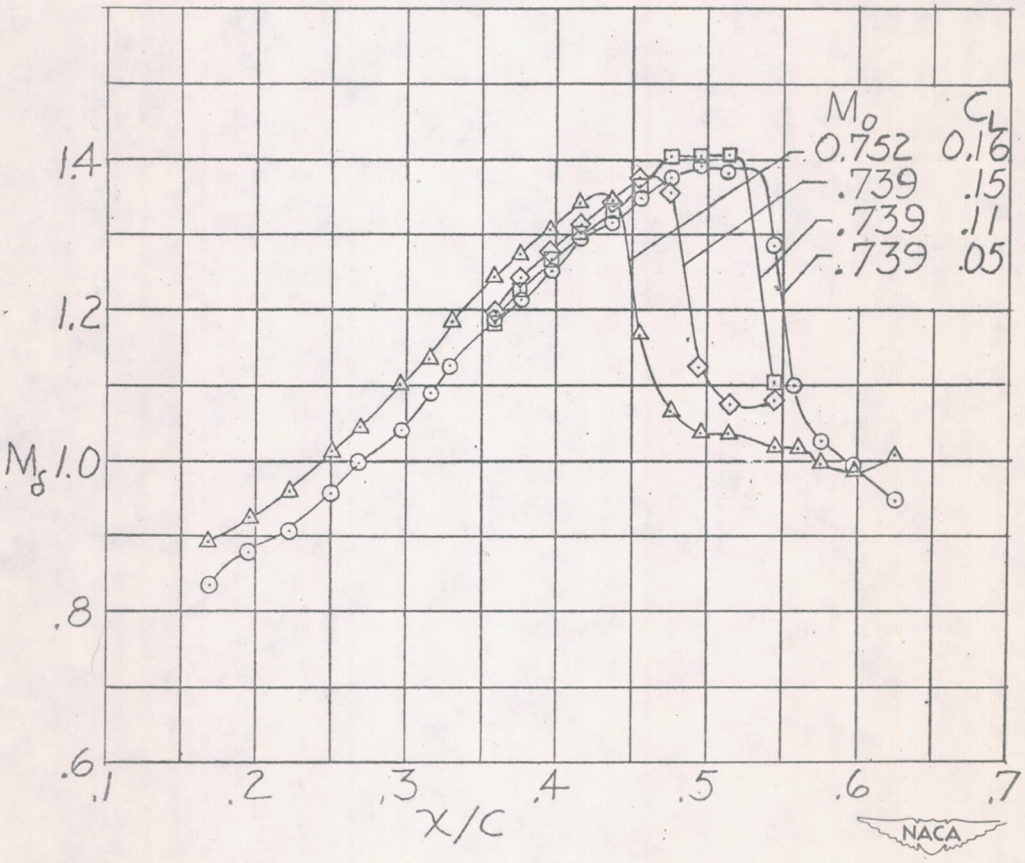

Figure 5.- Concluded.

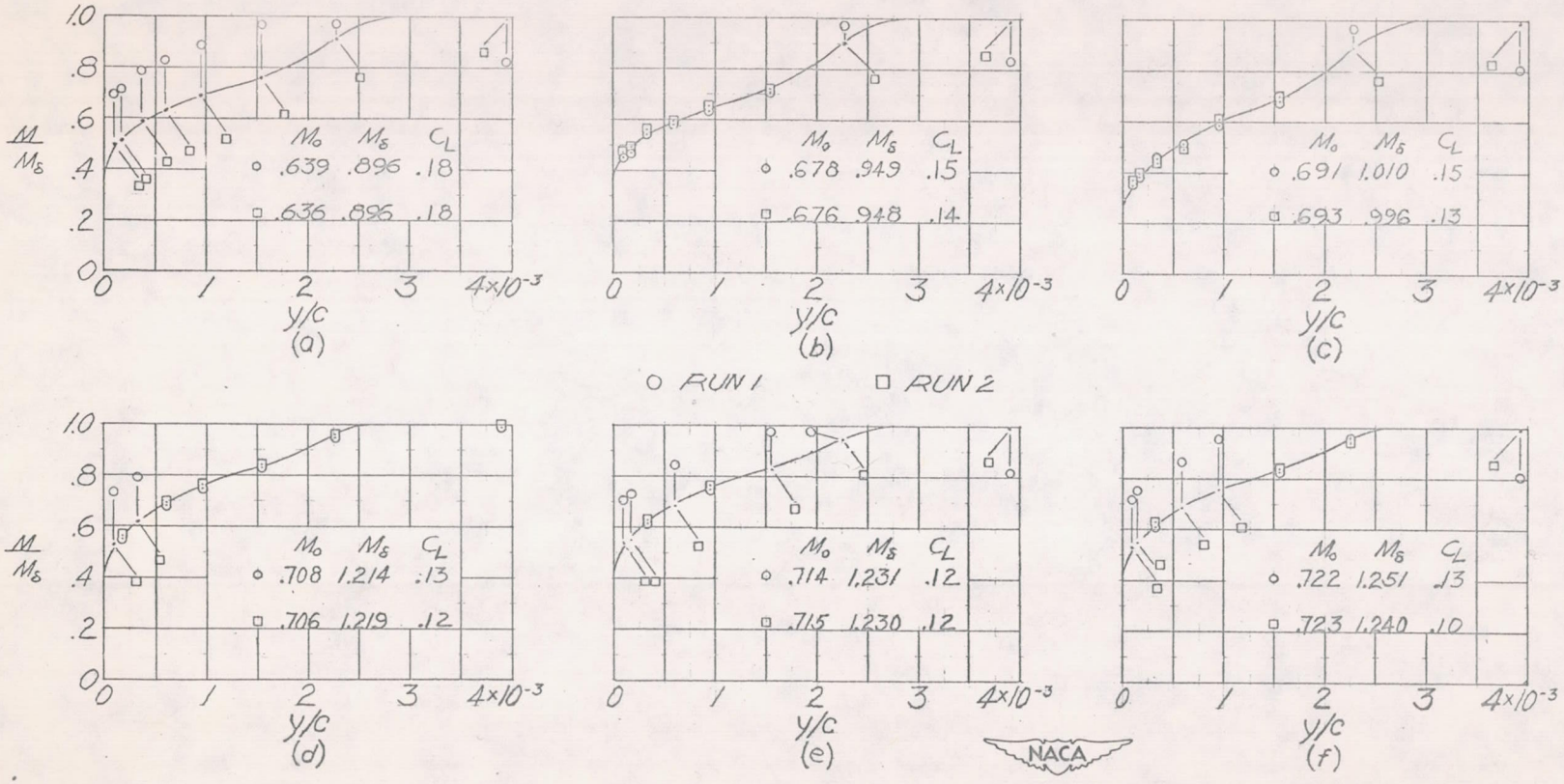

Figure 6.- Typical distribution of Mach number through the boundary layer on contour A at various Mach numbers M_o. $\frac{x}{c} = 0.419$.

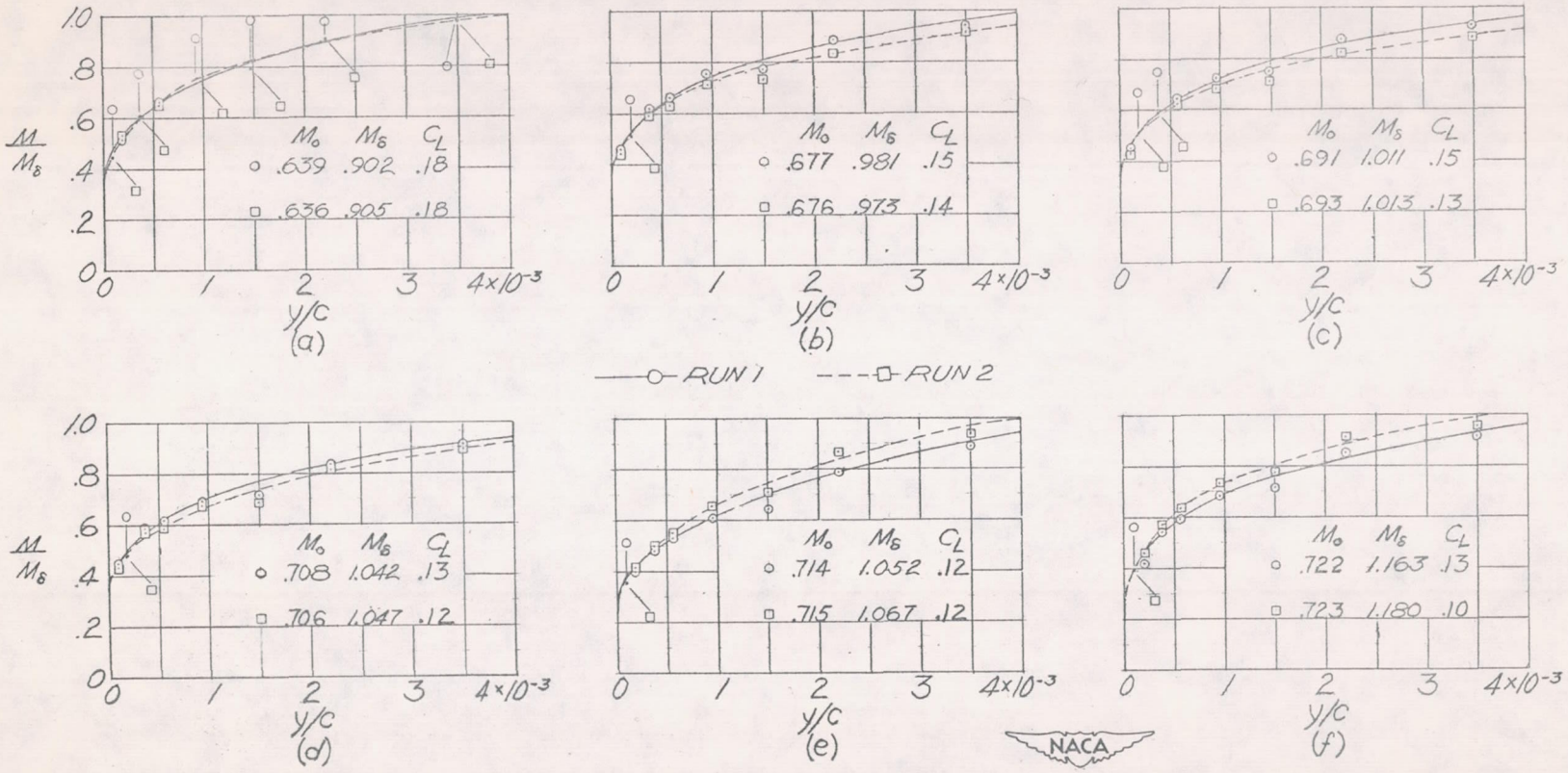

Figure 7.- Typical distribution of Mach number through the boundary layer on contour A at various Mach numbers M_o. $\frac{x}{c} = 0.520$.

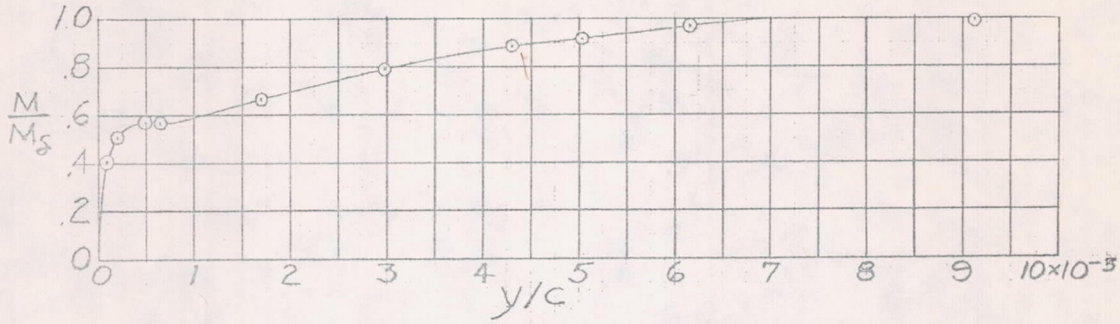

(a) $M_o = 0.620$; $M_\delta = 0.799$; $C_L = 0.20$.

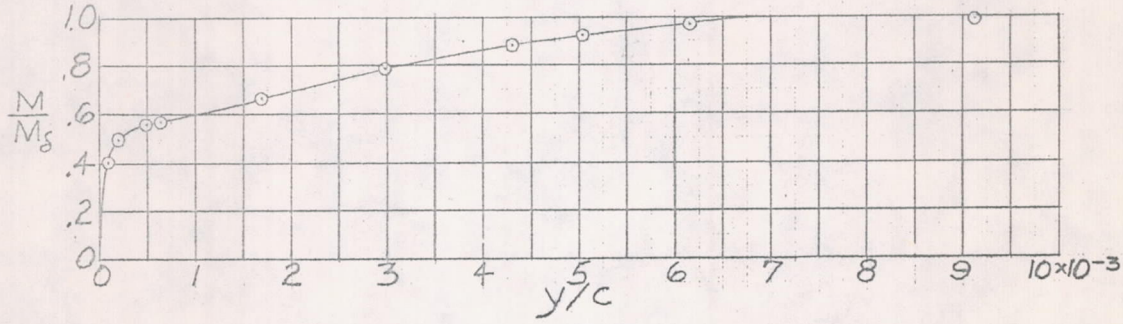

(b) $M_o = 0.640$; $M_\delta = 0.830$; $C_L = 0.20$.

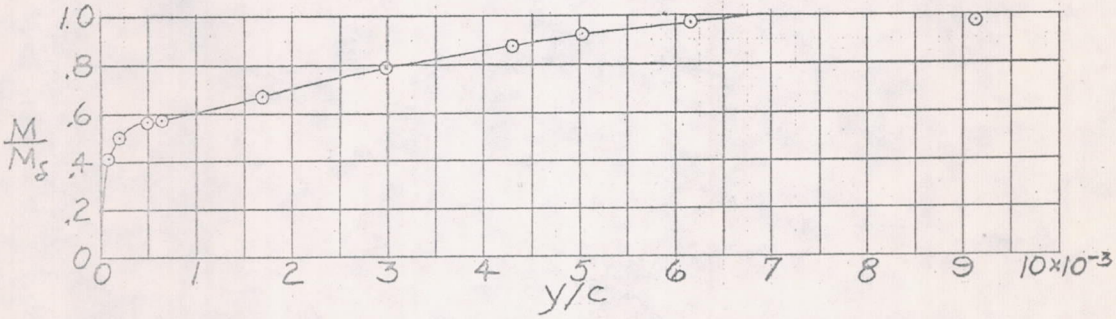

(c) $M_o = 0.660$; $M_\delta = 0.858$; $C_L = 0.15$.

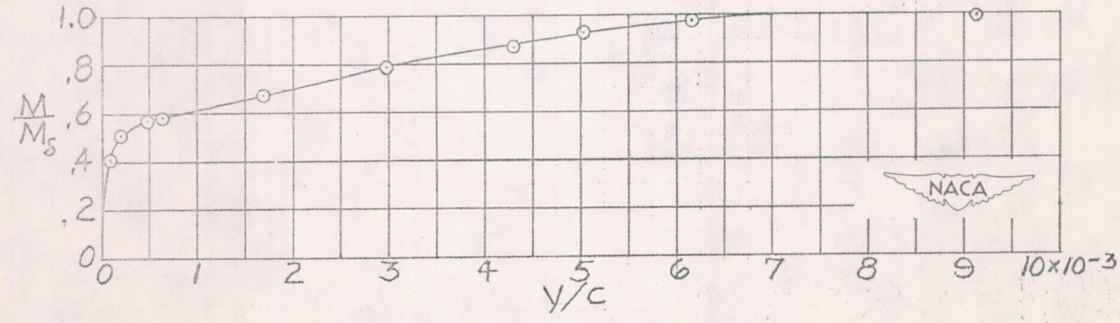

(d) $M_o = 0.680$; $M_\delta = 0.885$; $C_L = 0.14$.

Figure 8.- Typical variation of Mach number through the boundary layer on contour A. $\frac{x}{c} = 0.625$.

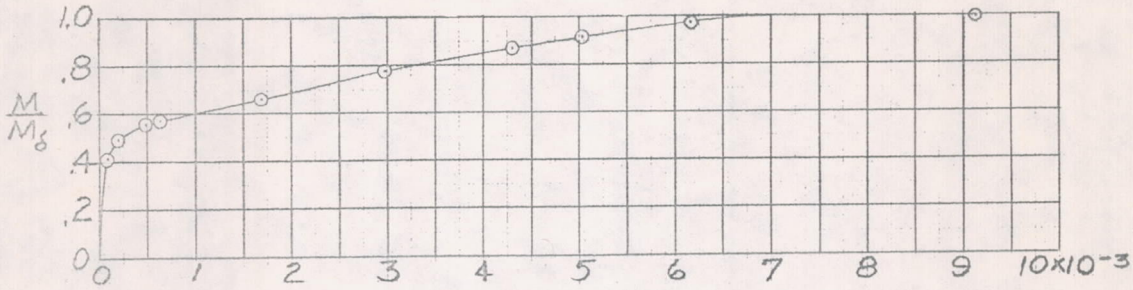

(e) $M_o = 0.700$; $M_\delta = 0.914$; $C_L = 0.12$.

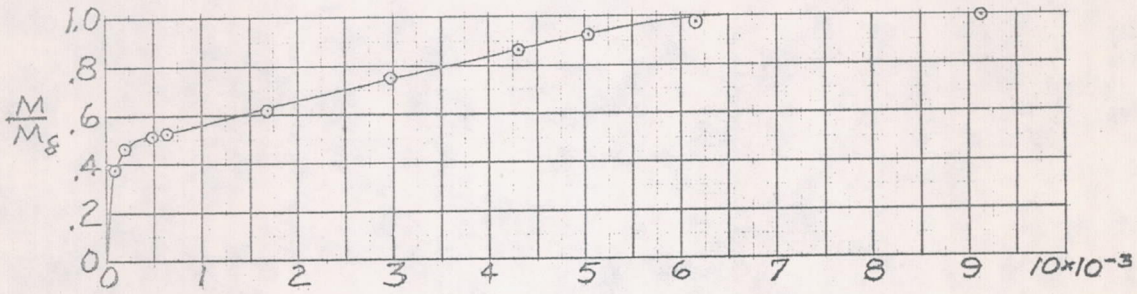

(f) $M_o = 0.710$; $M_\delta = 0.926$; $C_L = 0.11$.

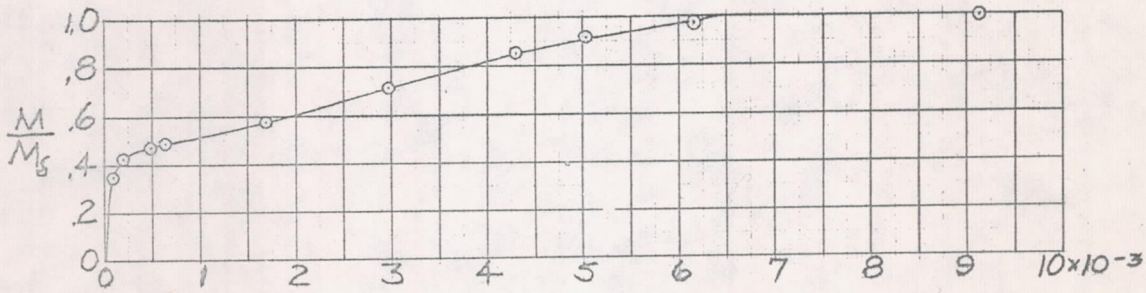

(g) $M_o = 0.720$; $M_\delta = 0.936$; $C_L = 0.10$.

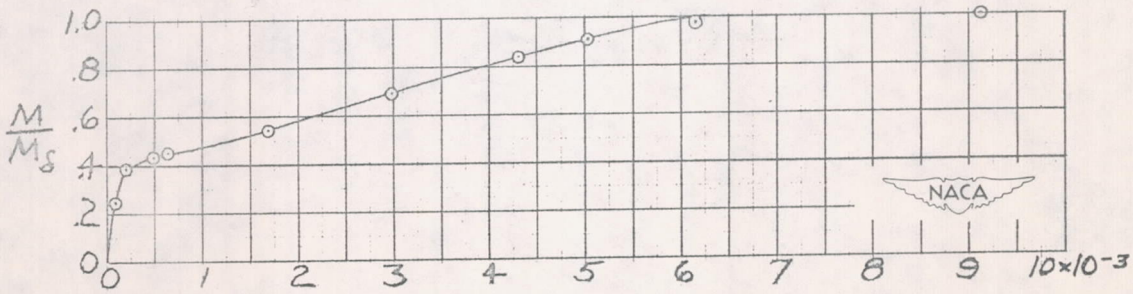

(h) $M_o = 0.723$; $M_\delta = 0.935$; $C_L = 0.10$.

Figure 8.- Continued.

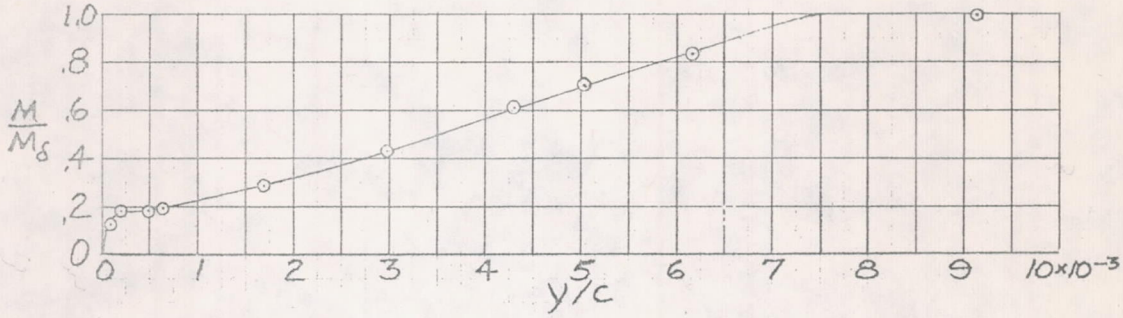

(i) $M_o = 0.731$; $M_\delta = 0.938$; $C_L = 0.13$.

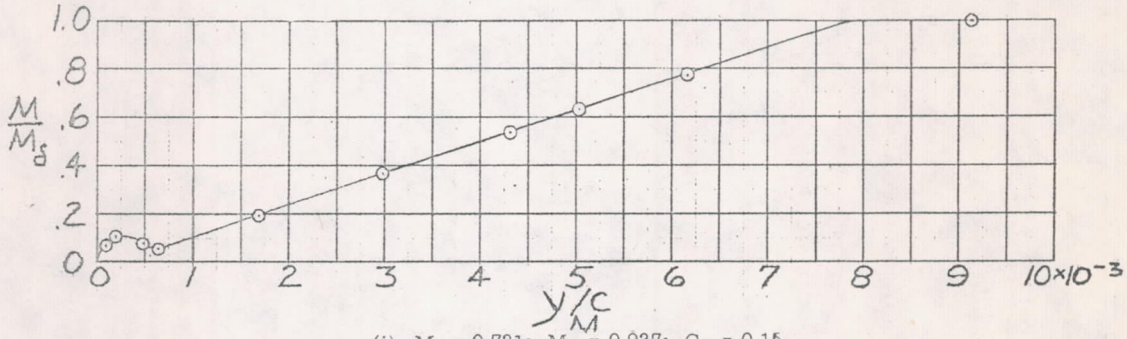

(j) $M_o = 0.731$; $M_\delta = 0.937$; $C_L = 0.15$.

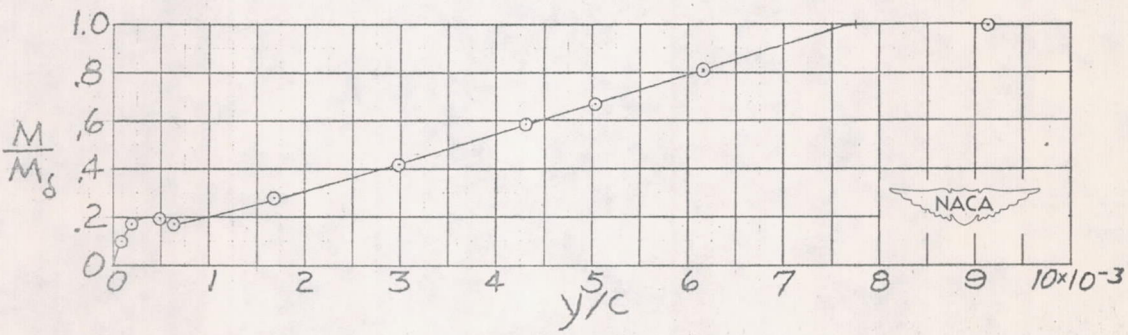

(k) $M_o = 0.724$; $M_\delta = 0.931$; $C_L = 0.19$.

Figure 8.- Concluded.

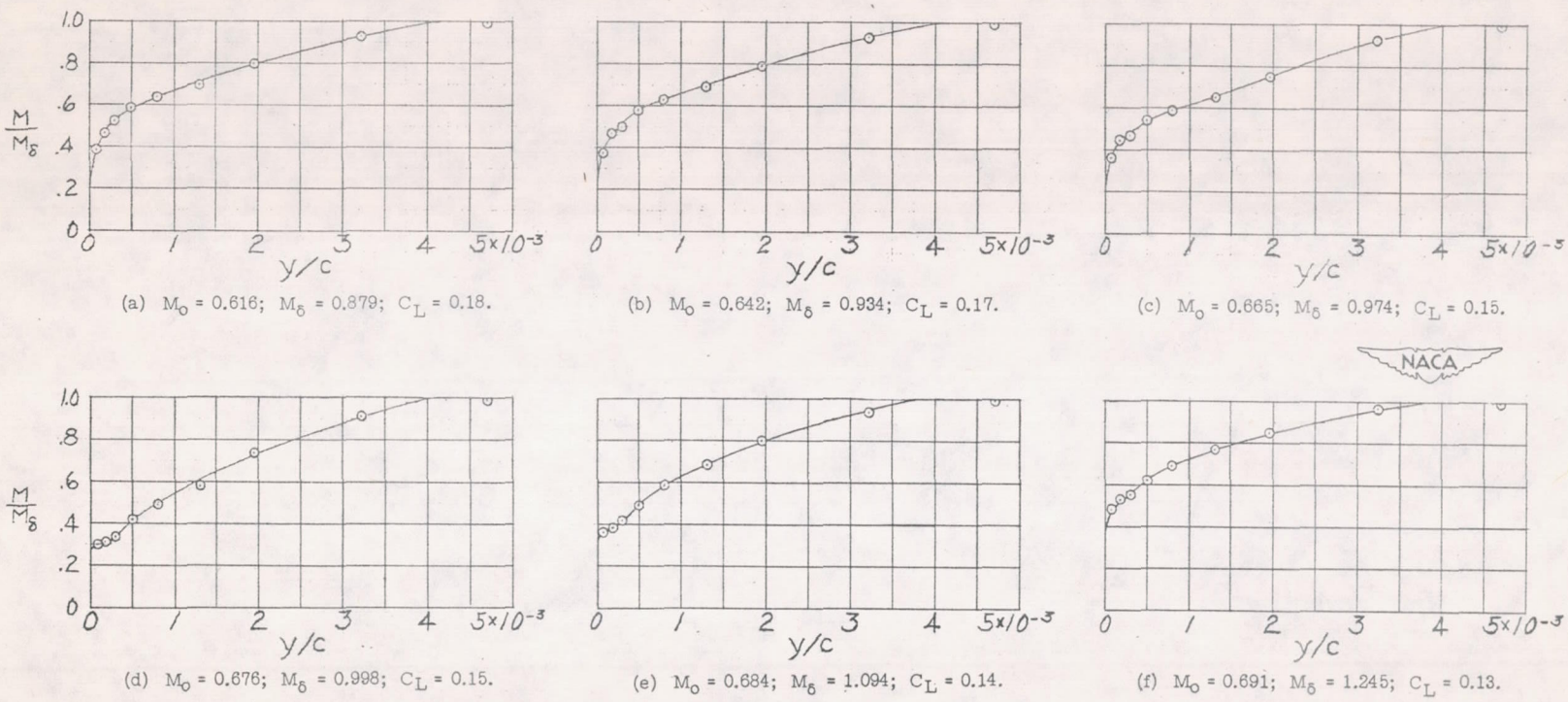

(a) $M_o = 0.616$; $M_\delta = 0.879$; $C_L = 0.18$.

(b) $M_o = 0.642$; $M_\delta = 0.934$; $C_L = 0.17$.

(c) $M_o = 0.665$; $M_\delta = 0.974$; $C_L = 0.15$.

(d) $M_o = 0.676$; $M_\delta = 0.998$; $C_L = 0.15$.

(e) $M_o = 0.684$; $M_\delta = 1.094$; $C_L = 0.14$.

(f) $M_o = 0.691$; $M_\delta = 1.245$; $C_L = 0.13$.

Figure 9.- Typical distribution of Mach number through the boundary layer on contour B at various Mach numbers M_o. $\frac{x}{c} = 0.456$.

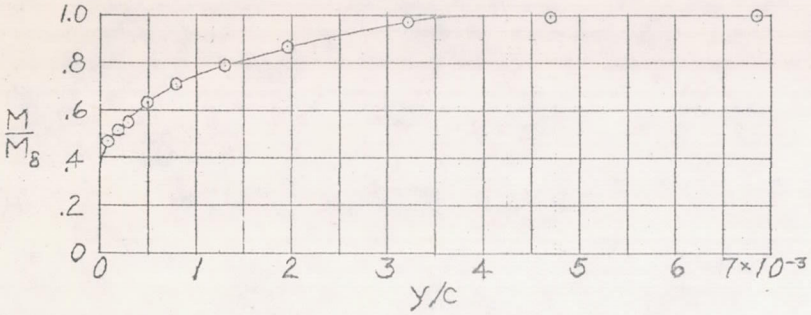

(g) $M_o = 0.714$; $M_\delta = 1.322$; $C_L = 0.12$.

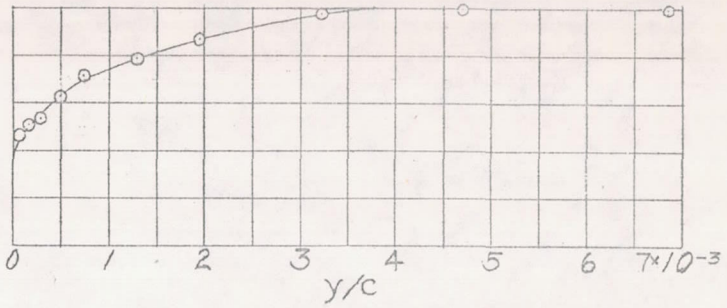

(h) $M_o = 0.741$; $M_\delta = 1.357$; $C_L = 0.09$.

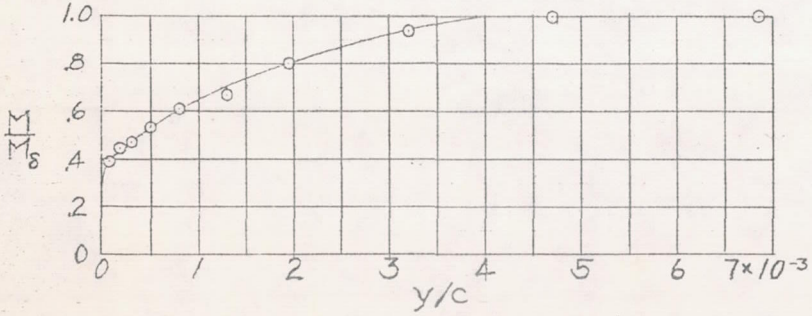

(i) $M_o = 0.741$; $M_\delta = 1.267$; $C_L = 0.19$.

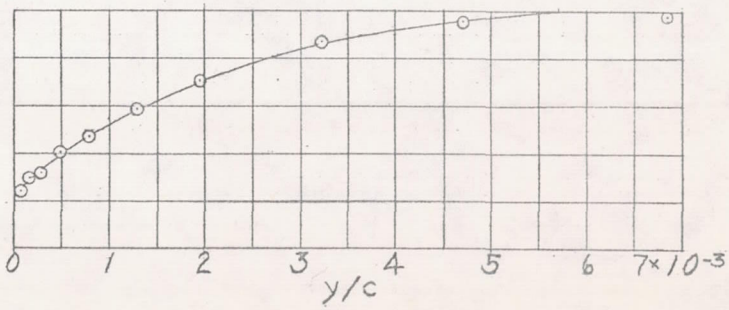

(j) $M_o = 0.742$; $M_\delta = 1.153$; $C_L = 0.22$.

Figure 9.- Concluded.

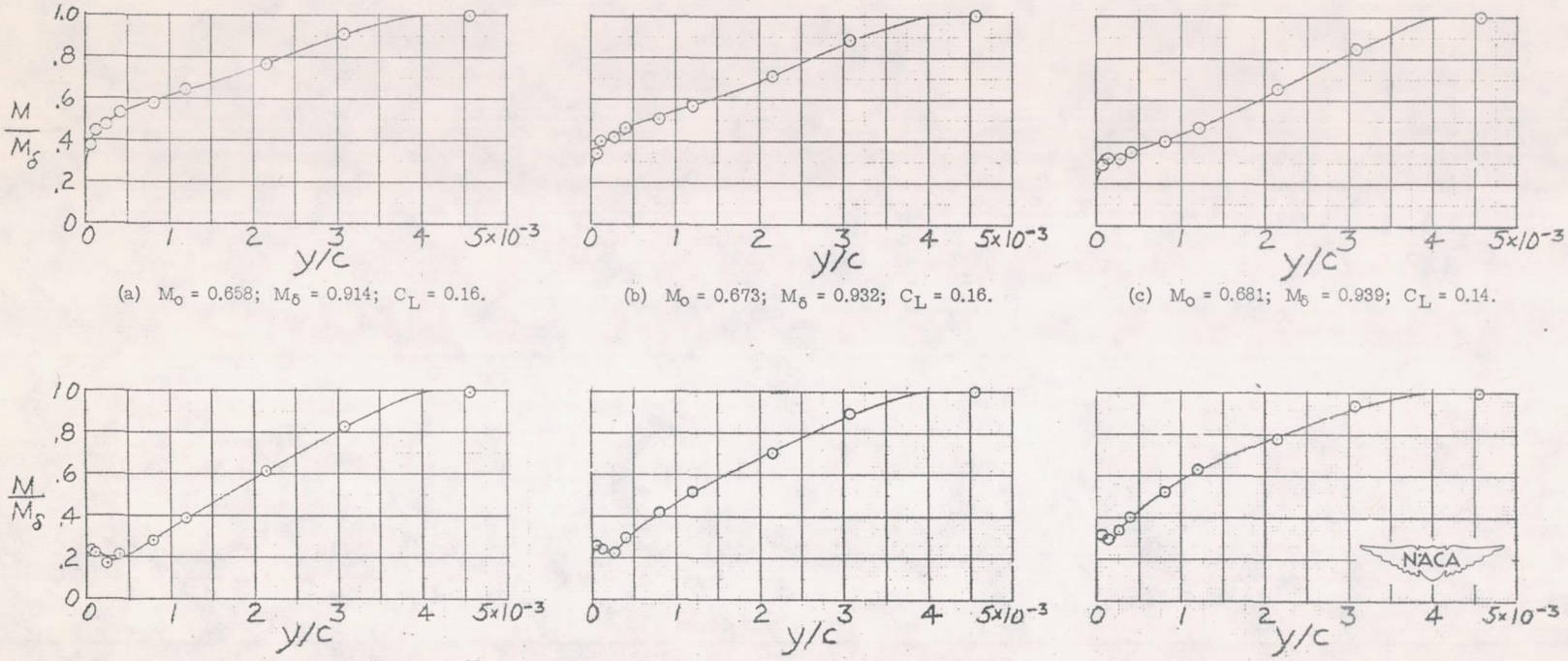

(a) $M_o = 0.658$; $M_\delta = 0.914$; $C_L = 0.16$.

(b) $M_o = 0.673$; $M_\delta = 0.932$; $C_L = 0.16$.

(c) $M_o = 0.681$; $M_\delta = 0.939$; $C_L = 0.14$.

(d) $M_o = 0.690$; $M_\delta = 0.975$; $C_L = 0.15$.

(e) $M_o = 0.694$; $M_\delta = 1.036$; $C_L = 0.12$.

(f) $M_o = 0.699$; $M_\delta = 1.087$; $C_L = 0.12$.

Figure 10.- Typical distribution of Mach number through the boundary layer on contour B at various Mach numbers M_o. $\frac{x}{c} = 0.496$.

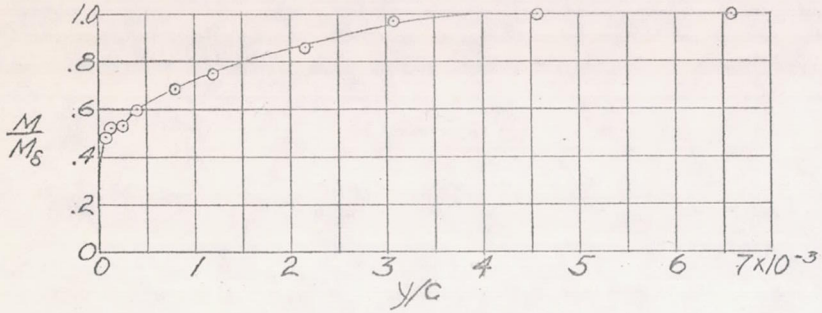

(g) $M_o = 0.714$; $M_\delta = 1.338$; $C_L = 0.12$.

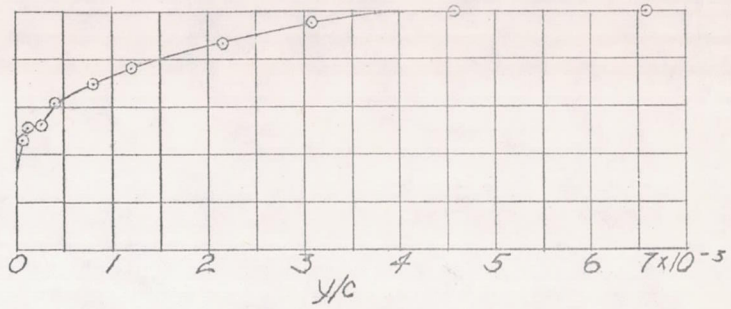

(h) $M_o = 0.733$; $M_\delta = 1.384$; $C_L = 0.18$.

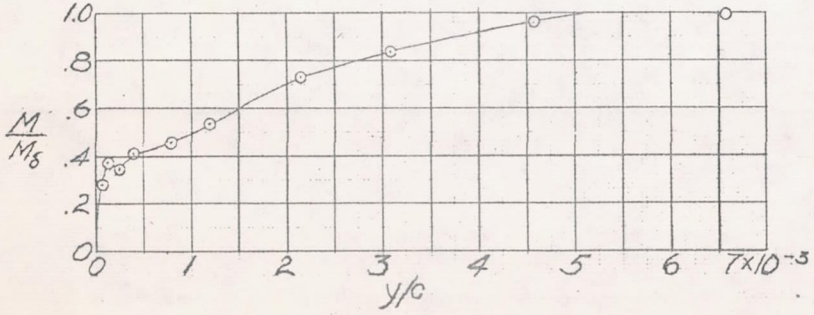

(i) $M_o = 0.734$; $M_\delta = 1.199$; $C_L = 0.19$.

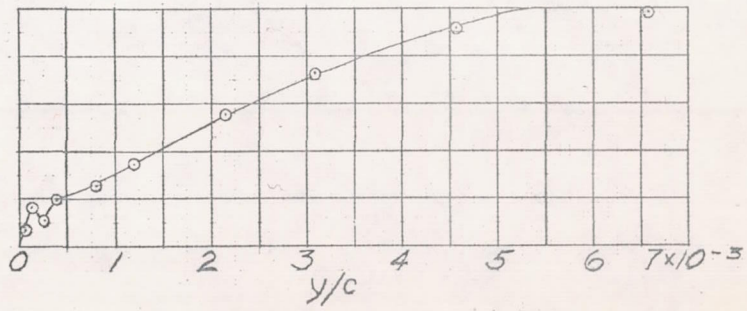

(j) $M_o = 0.735$; $M_\delta = 1.105$; $C_L = 0.19$.

Figure 10.- Concluded.

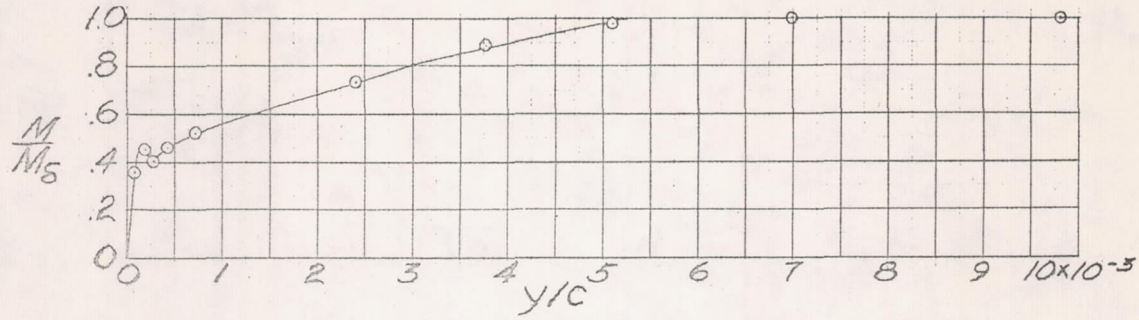

(a) $M_o = 0.659$; $M_\delta = 0.872$; $C_L = 0.15$.

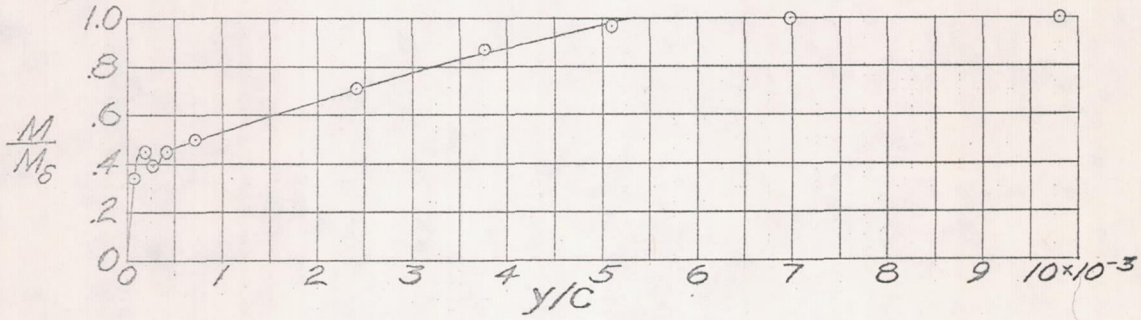

(b) $M_o = 0.673$; $M_\delta = 0.889$; $C_L = 0.14$.

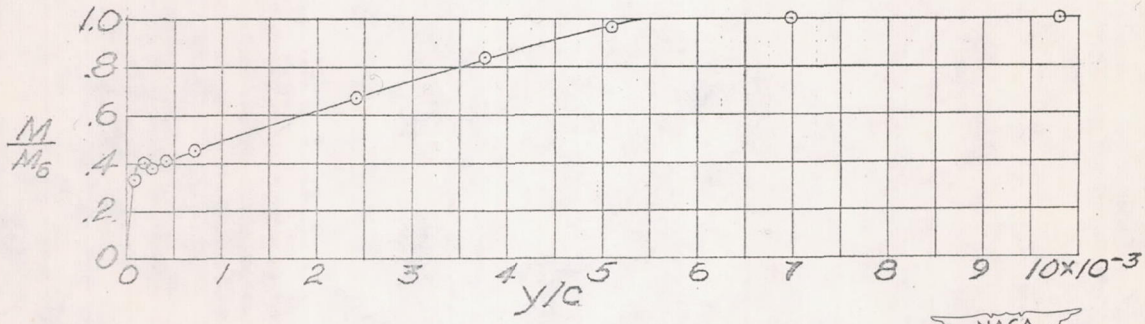

(c) $M_o = 0.680$; $M_\delta = 0.899$; $C_L = 0.15$.

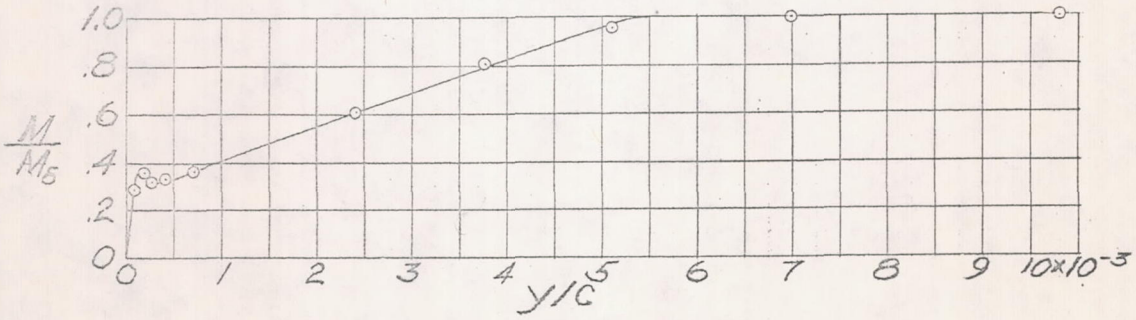

(d) $M_o = 0.690$; $M_\delta = 0.907$; $C_L = 0.13$.

Figure 11.- Typical distribution of Mach number through the boundary layer on contour B at various Mach numbers M_o. $\frac{x}{c} = 0.544$.

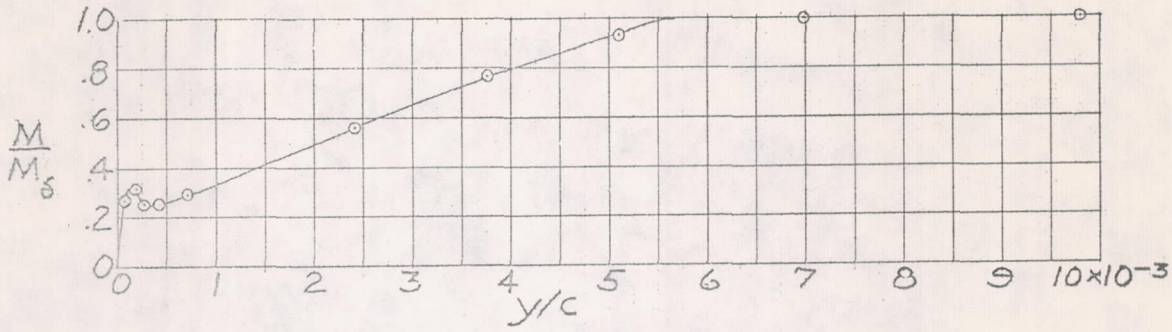

(e) $M_o = 0.694$; $M_\delta = 0.909$; $C_L = 0.14$.

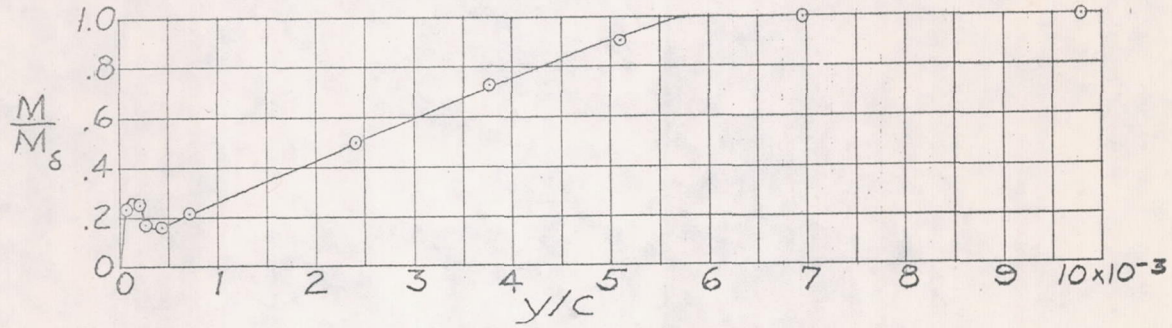

(f) $M_o = 0.700$; $M_\delta = 0.925$; $C_L = 0.13$.

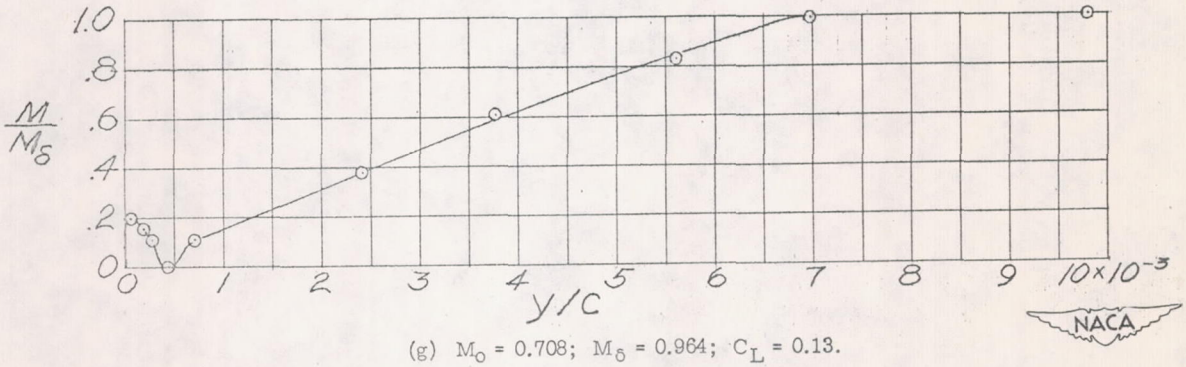

(g) $M_o = 0.708$; $M_\delta = 0.964$; $C_L = 0.13$.

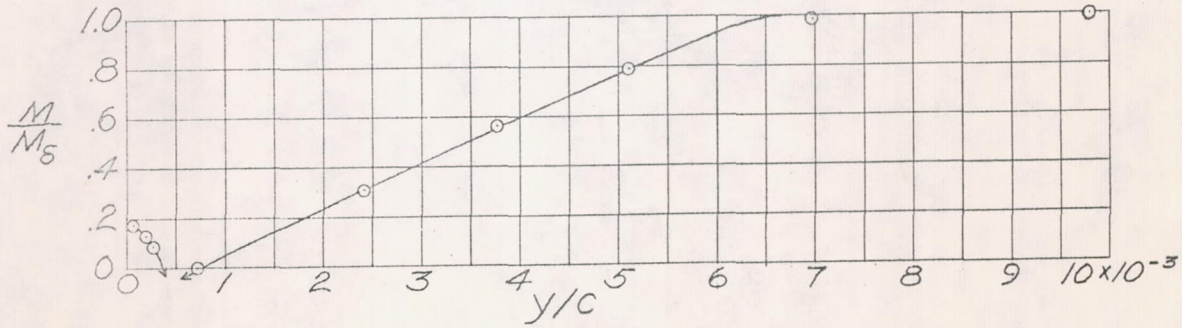

(h) $M_o = 0.713$; $M_\delta = 1.004$; $C_L = 0.11$.

Figure 11.- Continued.

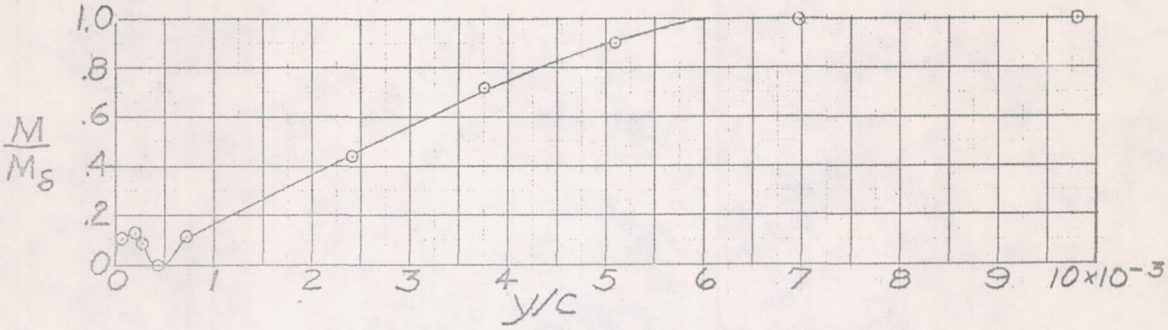

(i) $M_o = 0.733$; $M_\delta = 1.087$; $C_L = 0.12$.

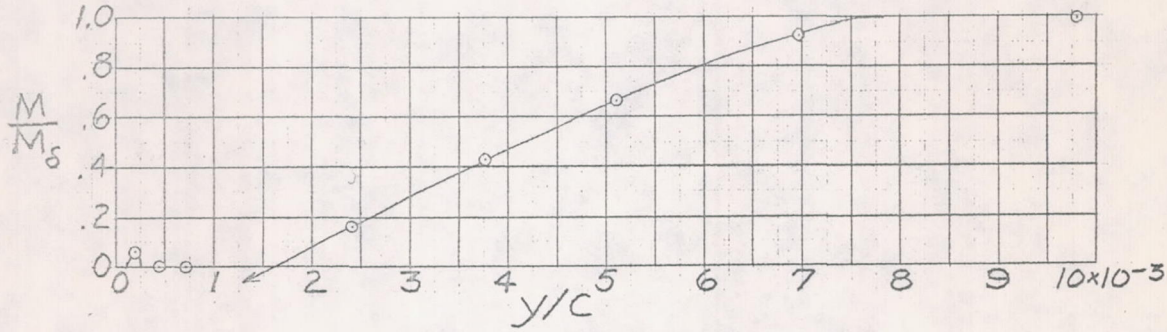

(j) $M_o = 0.738$; $M_\delta = 1.062$; $C_L = 0.13$.

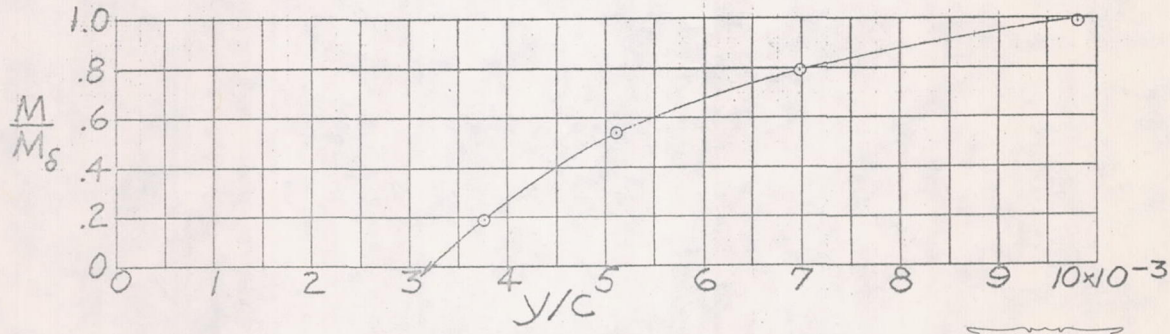

(k) $M_o = 0.739$; $M_\delta = 1.052$; $C_L = 0.13$

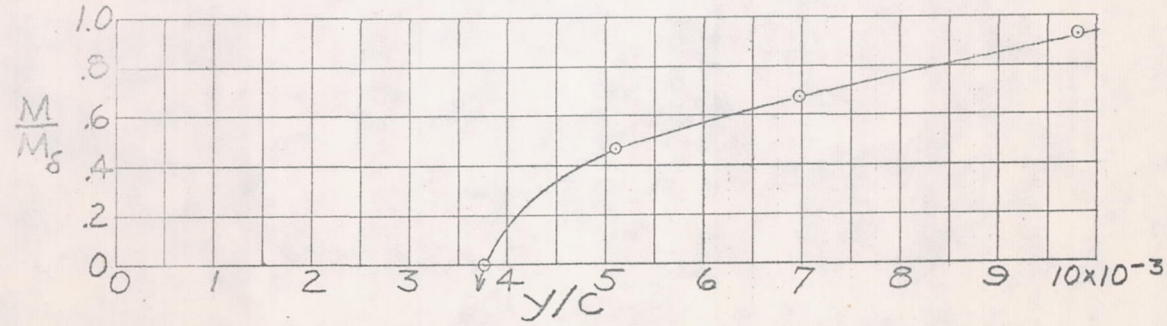

(l) $M_o = 0.740$; $M_\delta = 1.048$; $C_L = 0.13$.

Figure 11.- Concluded.

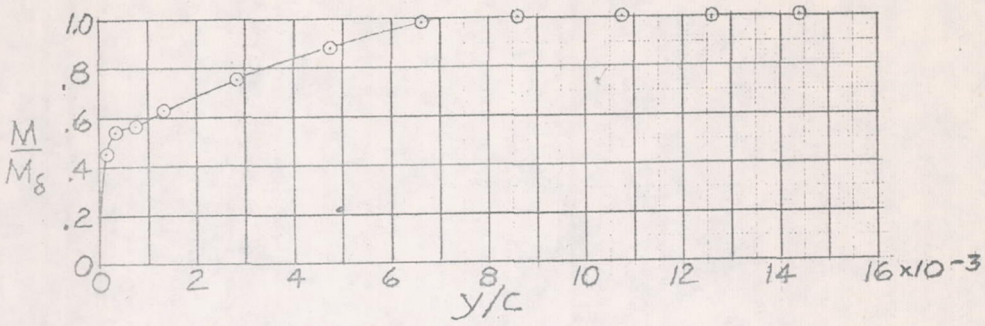

(a) $M_o = 0.620$; $M_\delta = 0.770$; $C_L = 0.19$.

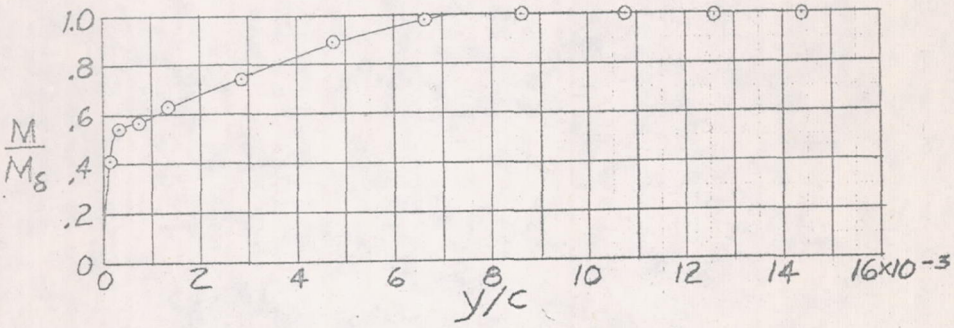

(b) $M_o = 0.640$; $M_\delta = 0.795$; $C_L = 0.17$.

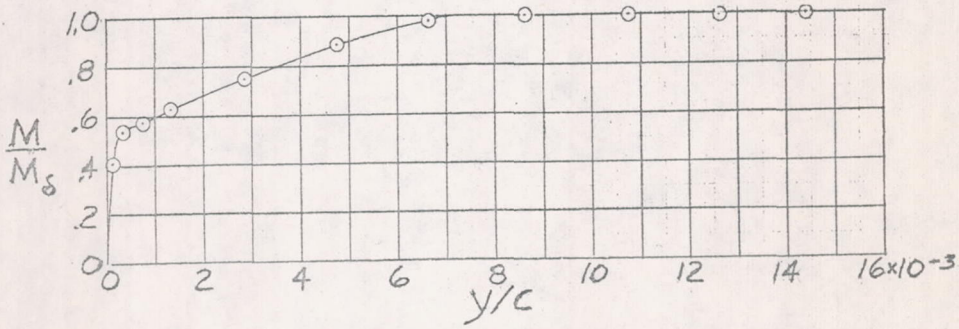

(c) $M_o = 0.660$; $M_\delta = 0.820$; $C_L = 0.15$.

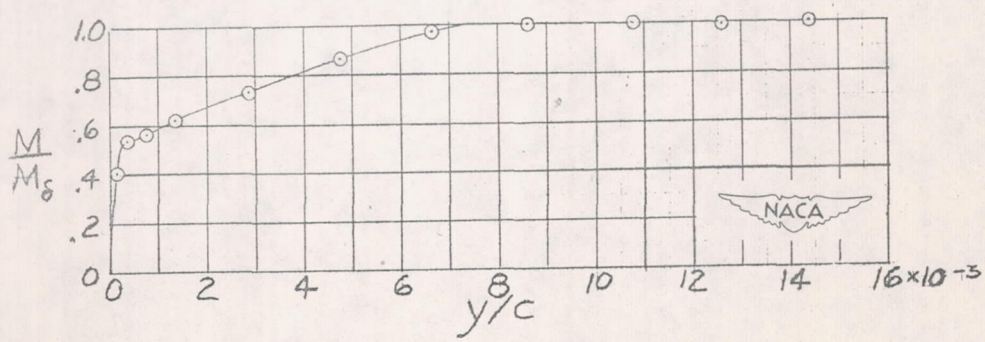

(d) $M_o = 0.677$; $M_\delta = 0.846$; $C_L = 0.14$.

Figure 12.- Typical distribution of Mach number through the boundary layer on contour B at various Mach numbers M_o. $\frac{X}{C} = 0.623$.

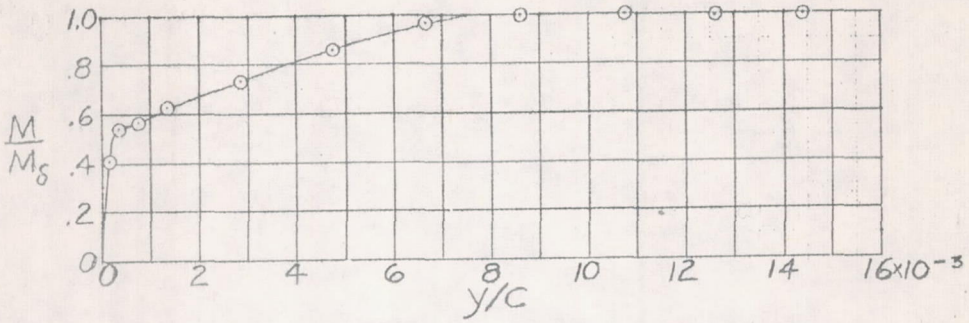

(e) $M_o = 0.680$; $M_\delta = 0.847$; $C_L = 0.14$.

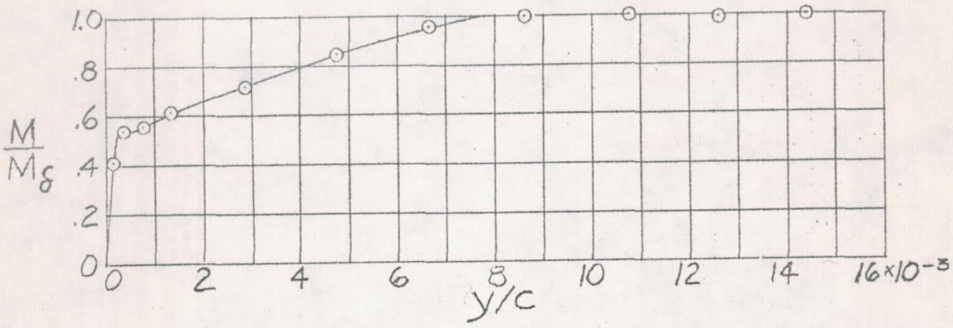

(f) $M_o = 0.690$; $M_\delta = 0.857$; $C_L = 0.14$.

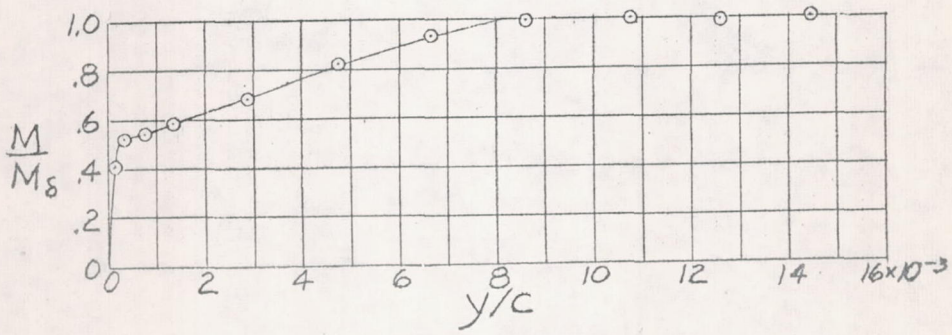

(g) $M_o = 0.700$; $M_\delta = 0.864$; $C_L = 0.13$.

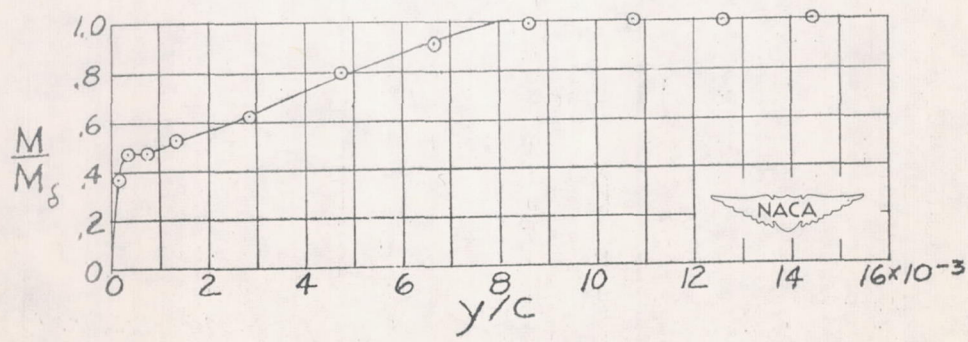

(h) $M_o = 0.710$; $M_\delta = 0.868$; $C_L = 0.12$.

Figure 12.- Continued.

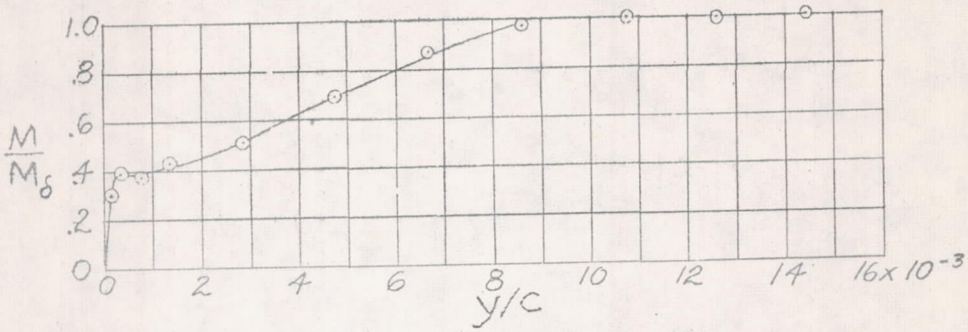

(i) $M_o = 0.717$; $M_\delta = 0.877$; $C_L = 0.11$.

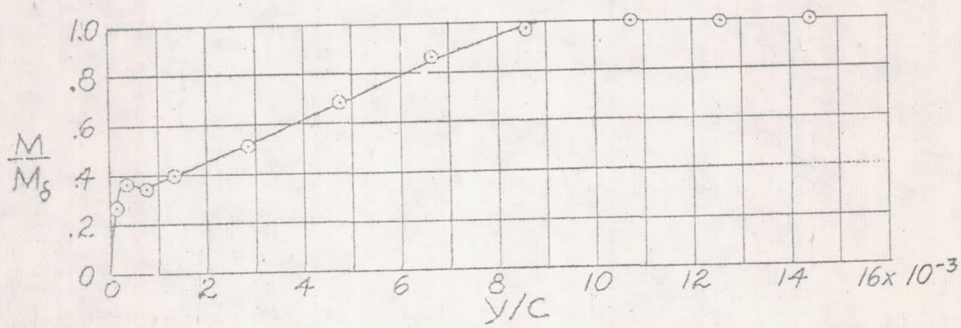

(j) $M_o = 0.720$; $M_\delta = 0.880$; $C_L = 0.11$.

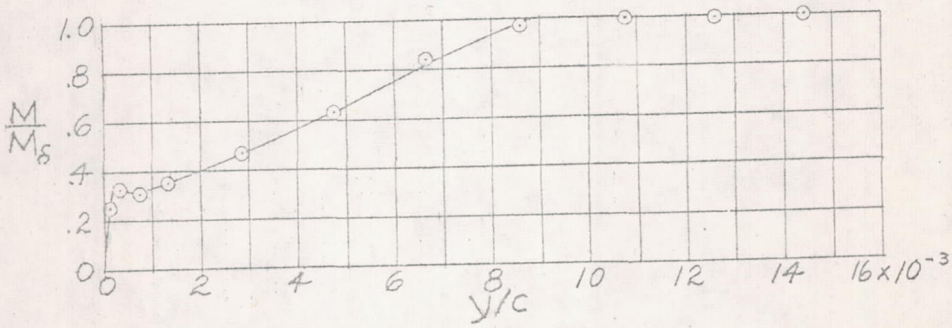

(k) $M_o = 0.723$; $M_\delta = 0.887$; $C_L = 0.11$.

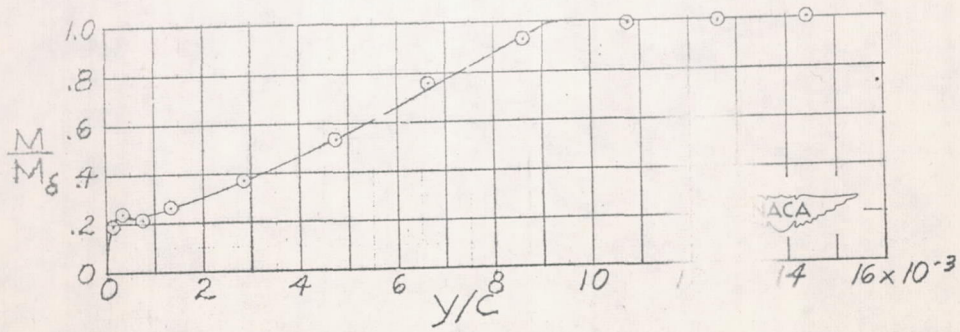

(l) $M_o = 0.729$; $M_\delta = 0.905$; $C_L = 0.0$

Figure 12.- Continued.

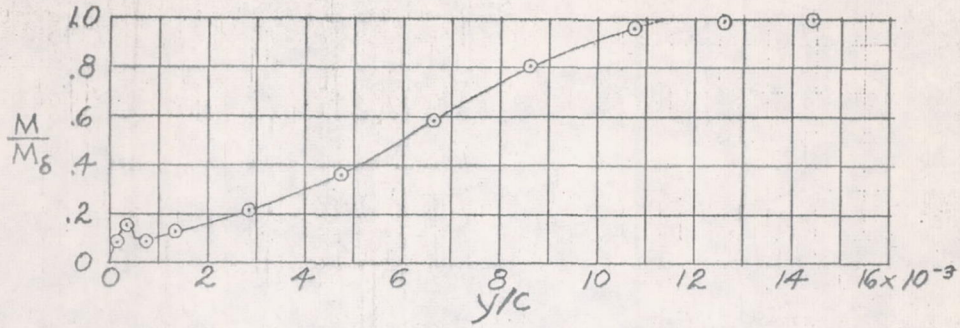

(m) $M_o = 0.731$; $M_\delta = 0.928$; $C_L = 0.13$.

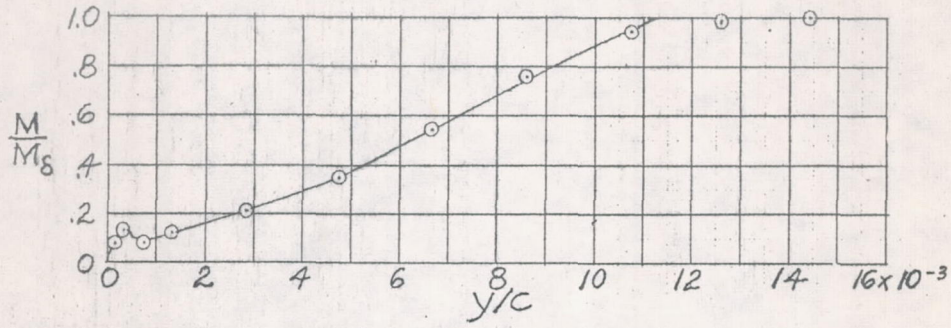

(n) $M_o = 0.733$; $M_\delta = 0.930$; $C_L = 0.13$.

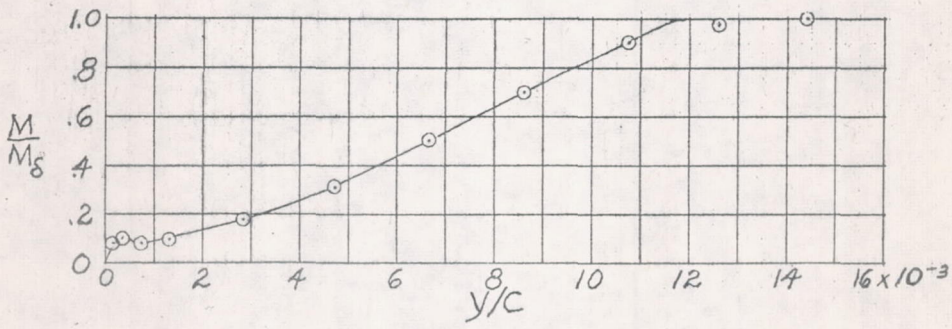

(o) $M_o = 0.733$; $M_\delta = 0.938$; $C_L = 0.15$.

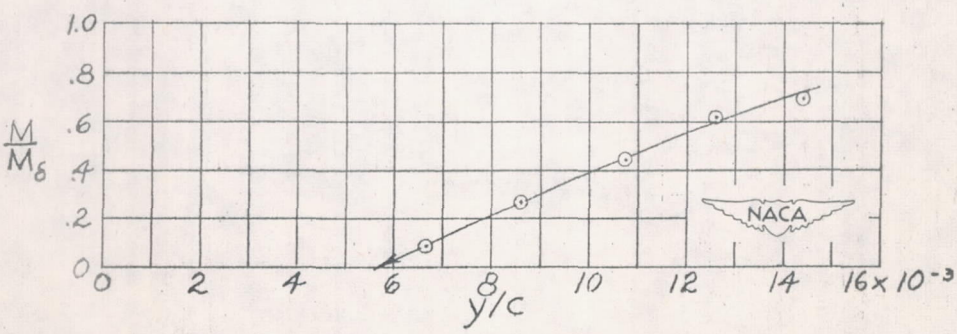

(p) $M_o = 0.735$; $M_\delta = 0.966$; $C_L = 0.18$.

Figure 12.- Concluded.

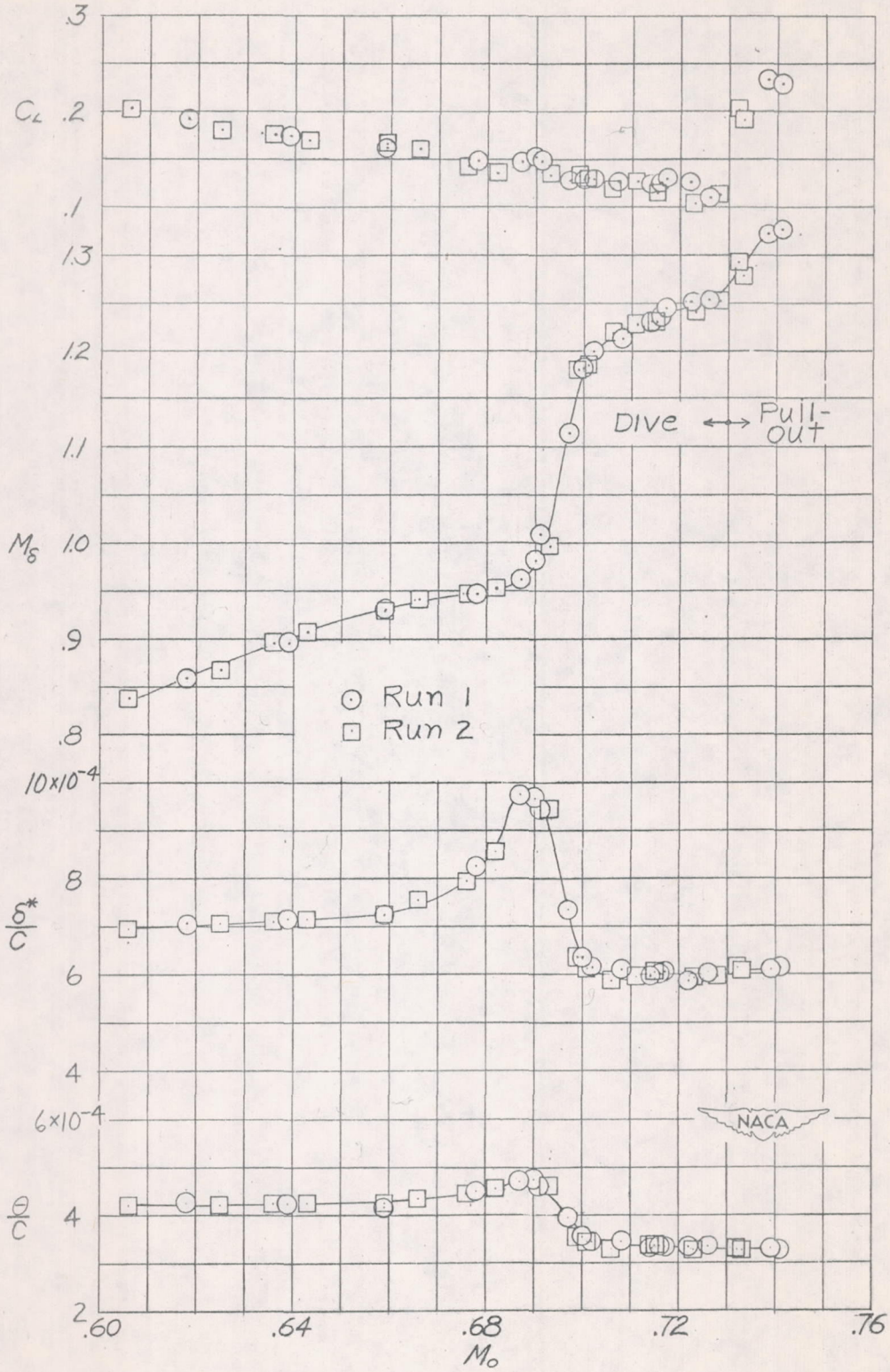

(a) $\frac{x}{c} = 0.419$.

Figure 13.- Variation with M_o of θ, δ^*, M_δ, and C_L. Contour A.

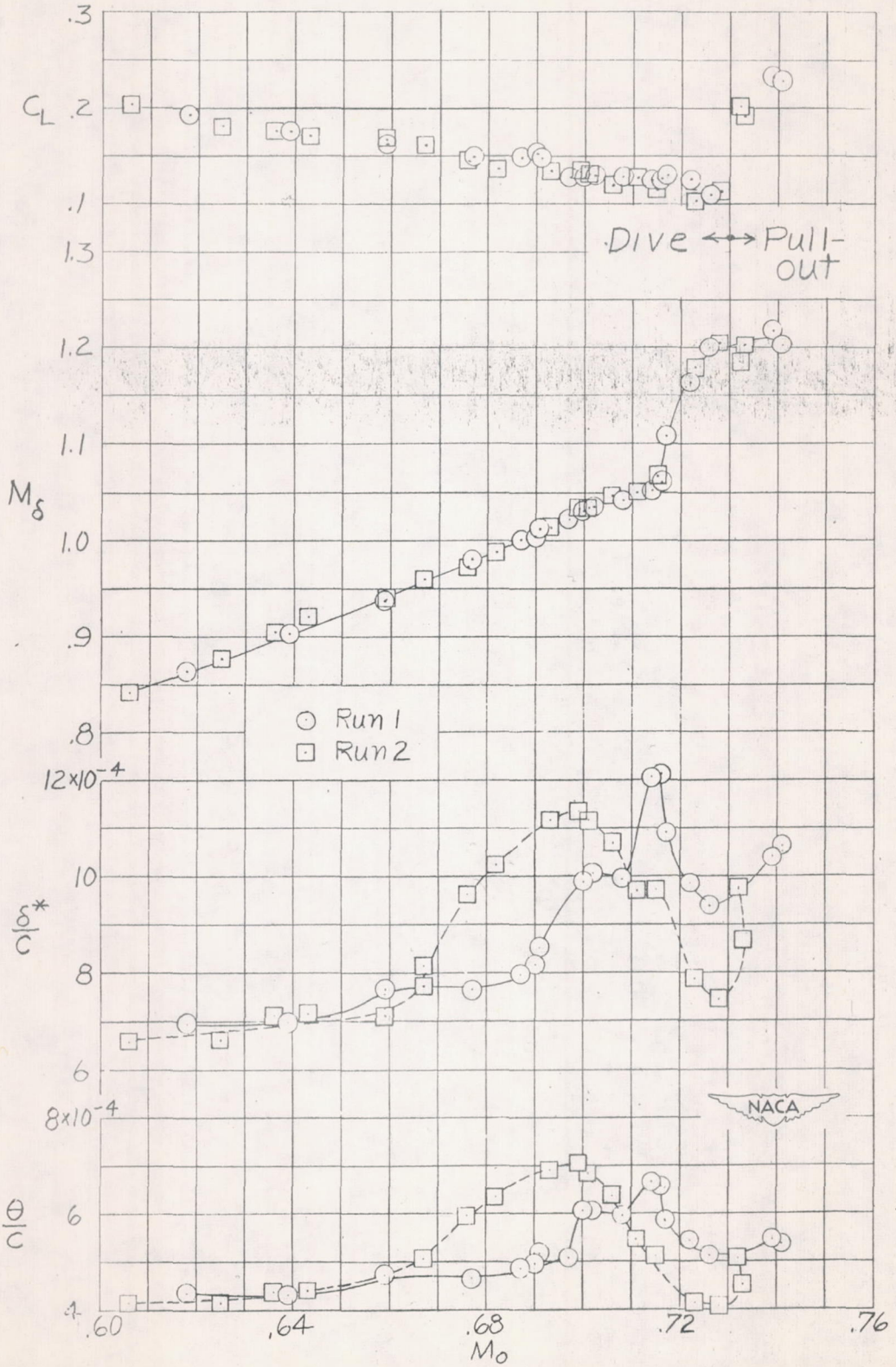

(b) $\frac{x}{c} = 0.520$.

Figure 13.- Continued.

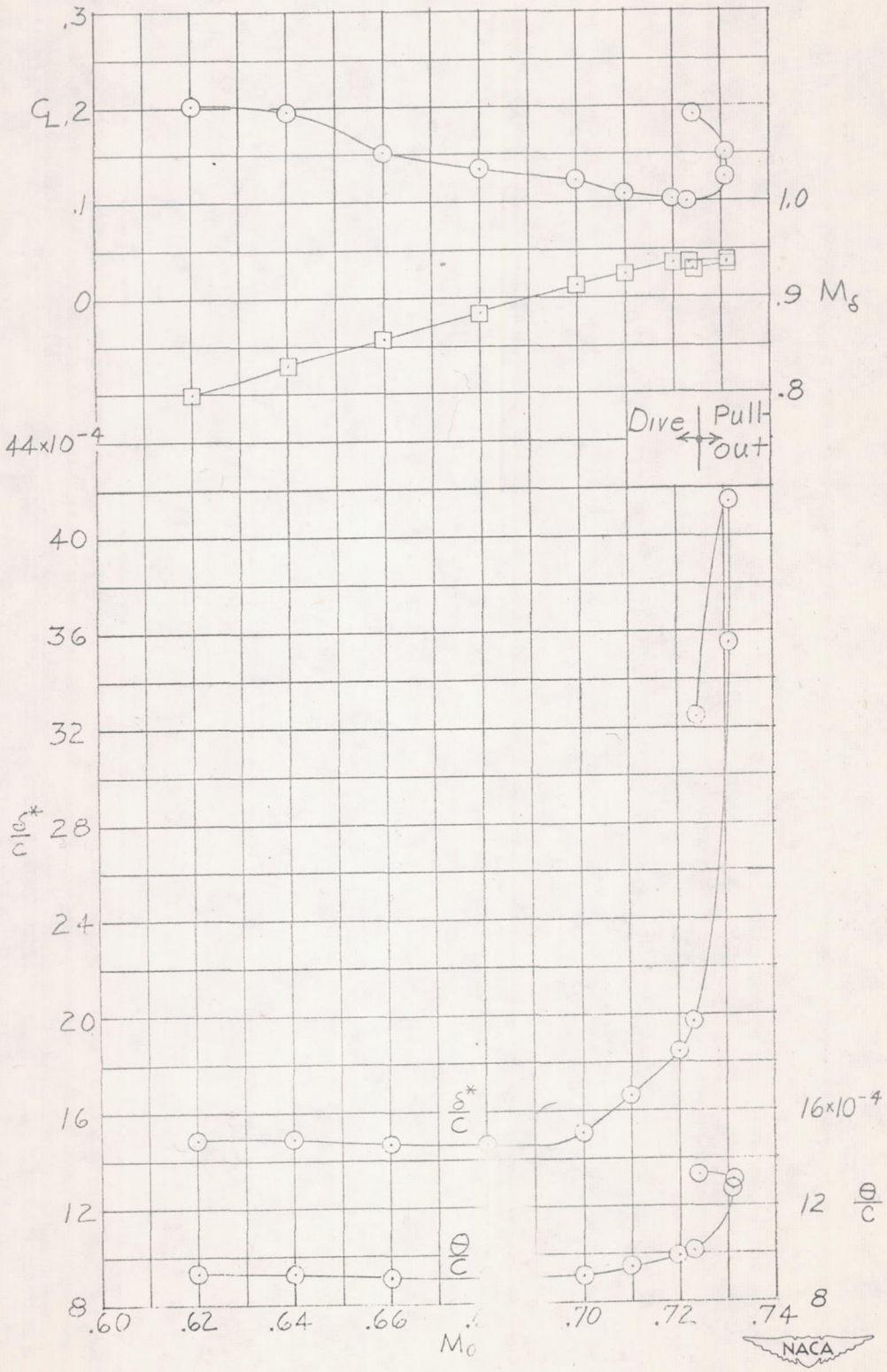

(c) $\frac{x}{c}$ =

Figure 13.- ded.

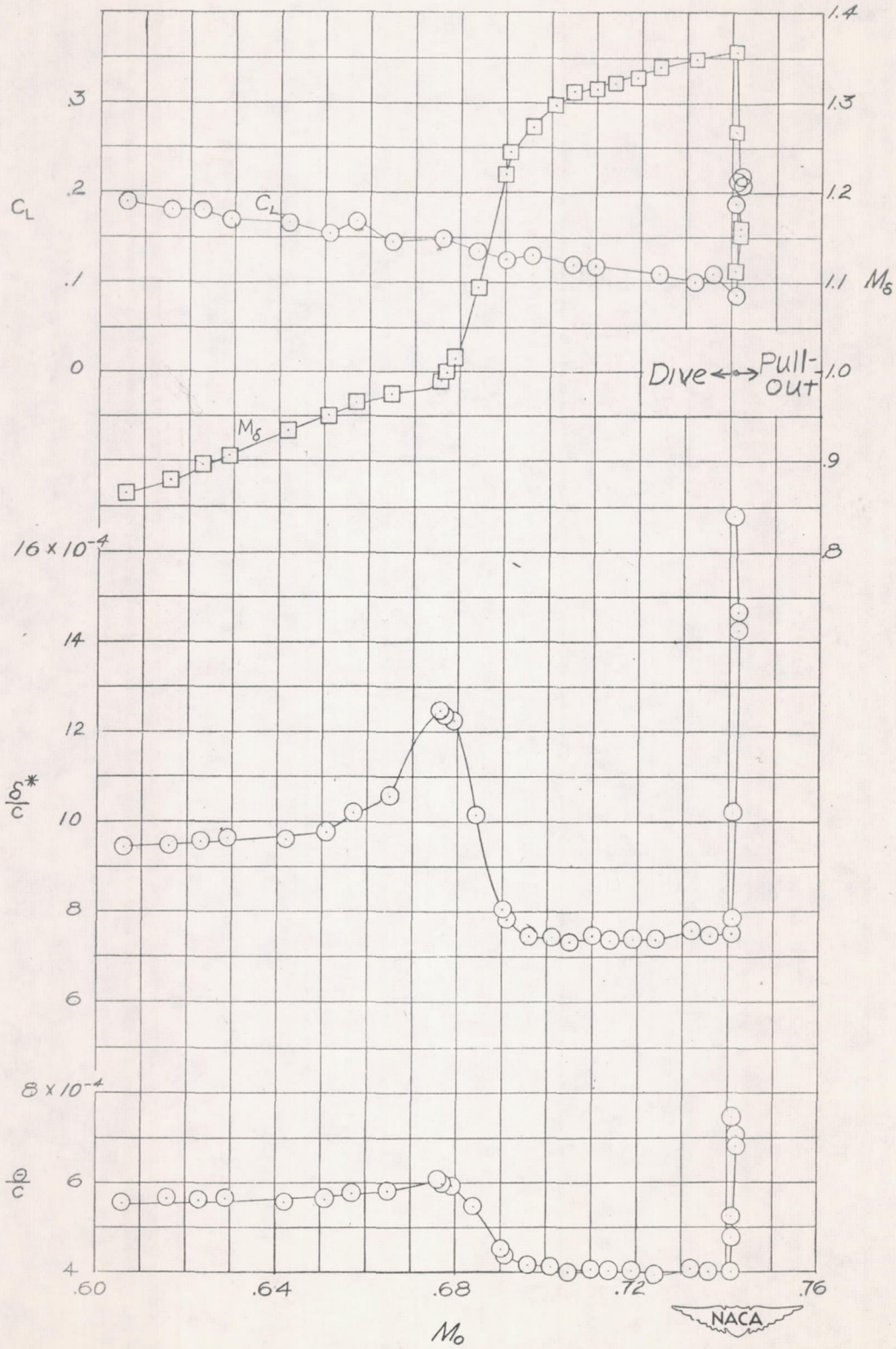

(a) $\frac{x}{c} = 0.456$.

Figure 14.- Variation with M_o of θ, δ^*, M_δ, and C_L. Contour B.

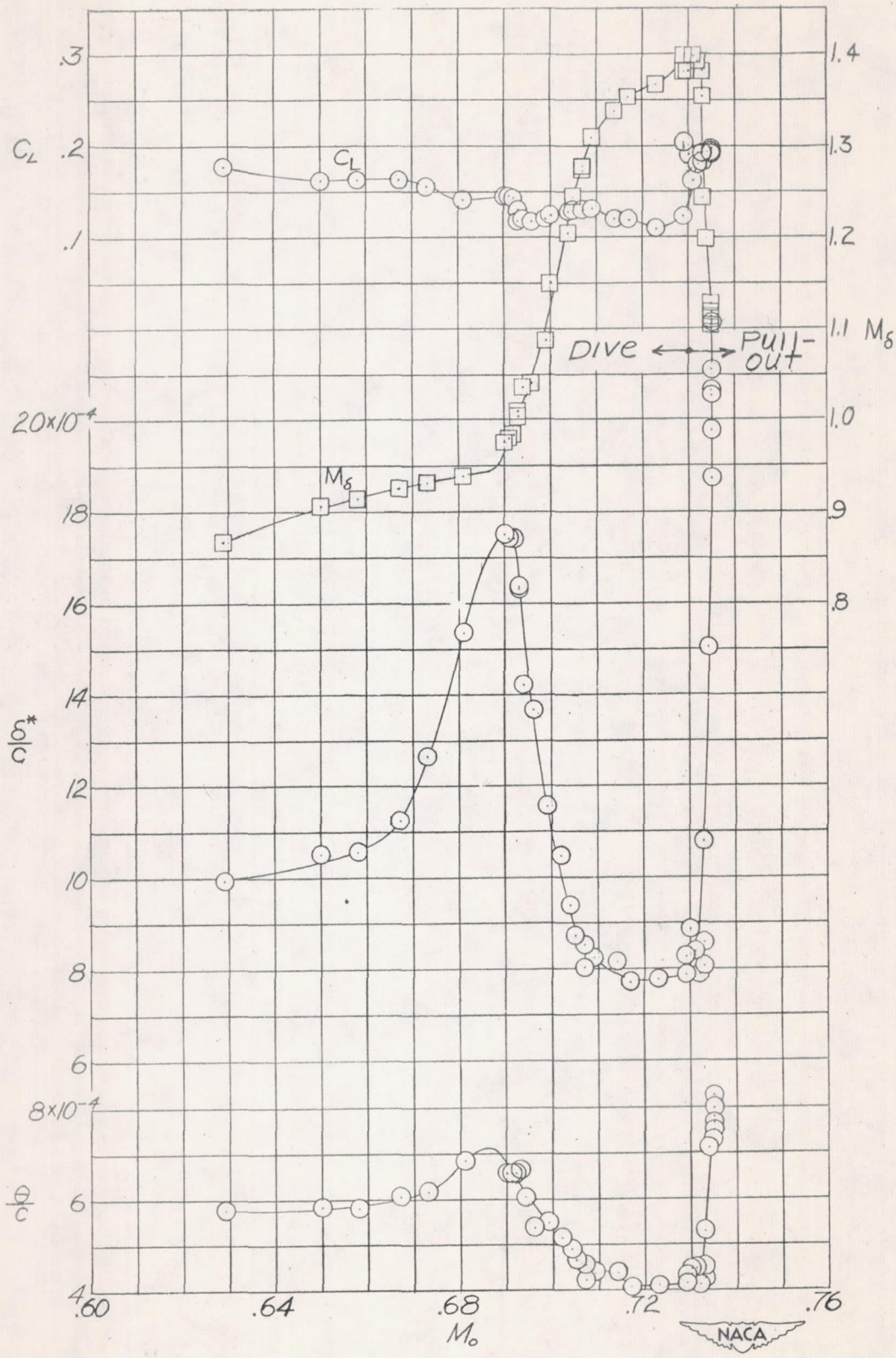

(b) $\frac{x}{c} = 0.496$.

Figure 14.- Continued.

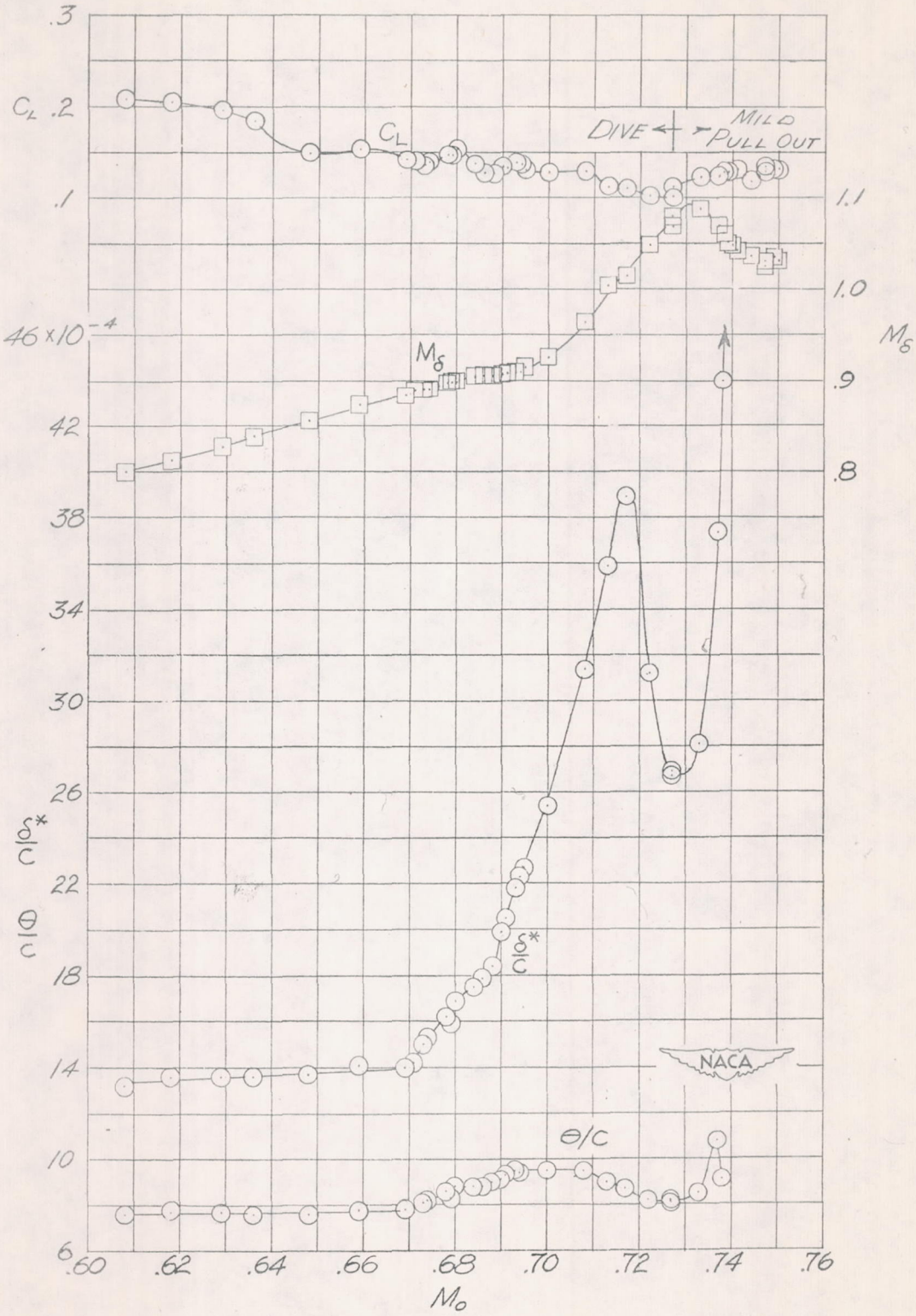

(c) $\frac{x}{c} = 0.544$.

Figure 14.- Continued.

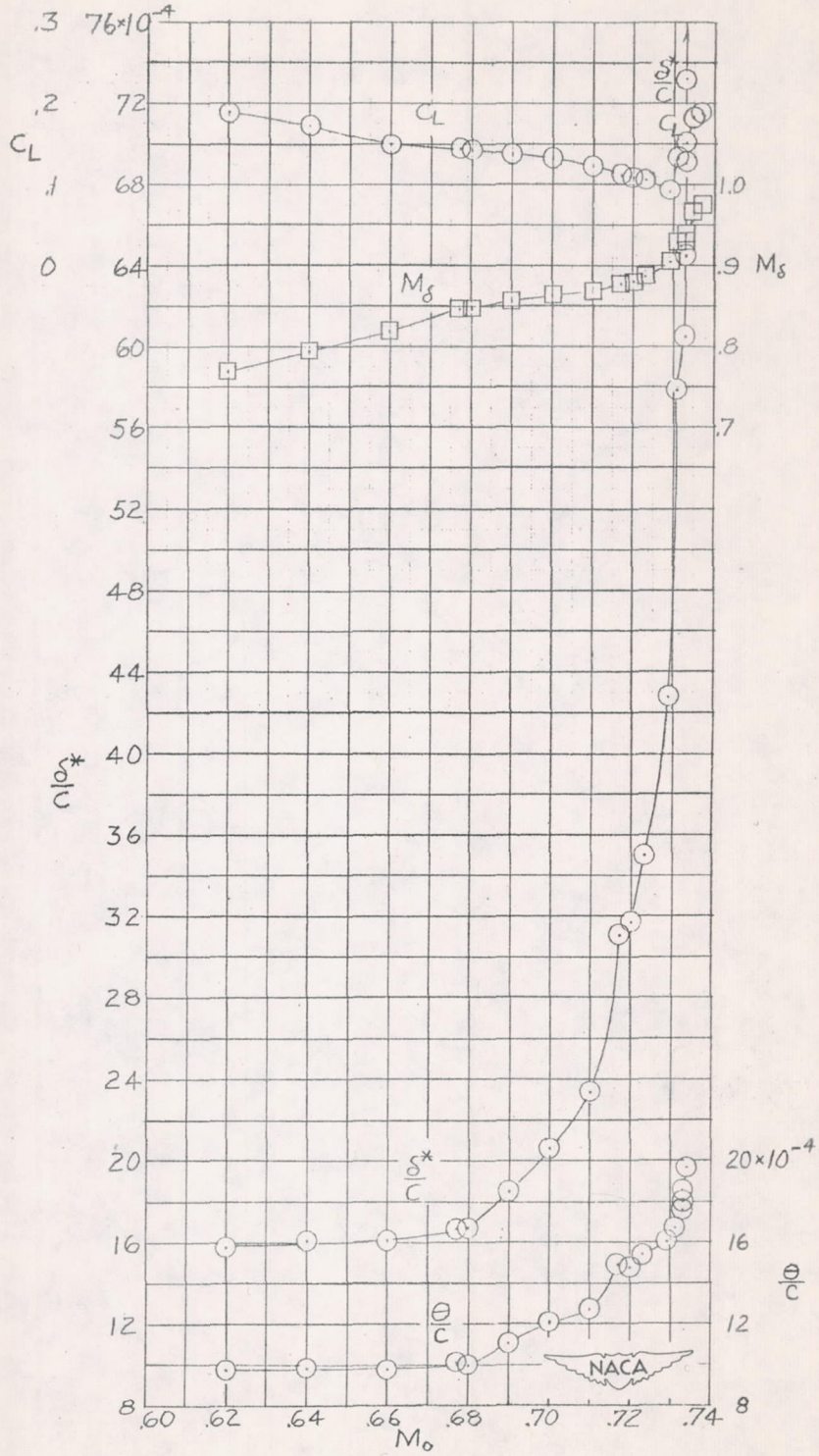

(d) $\frac{x}{c} = 0.623$.

Figure 14.- Concluded.

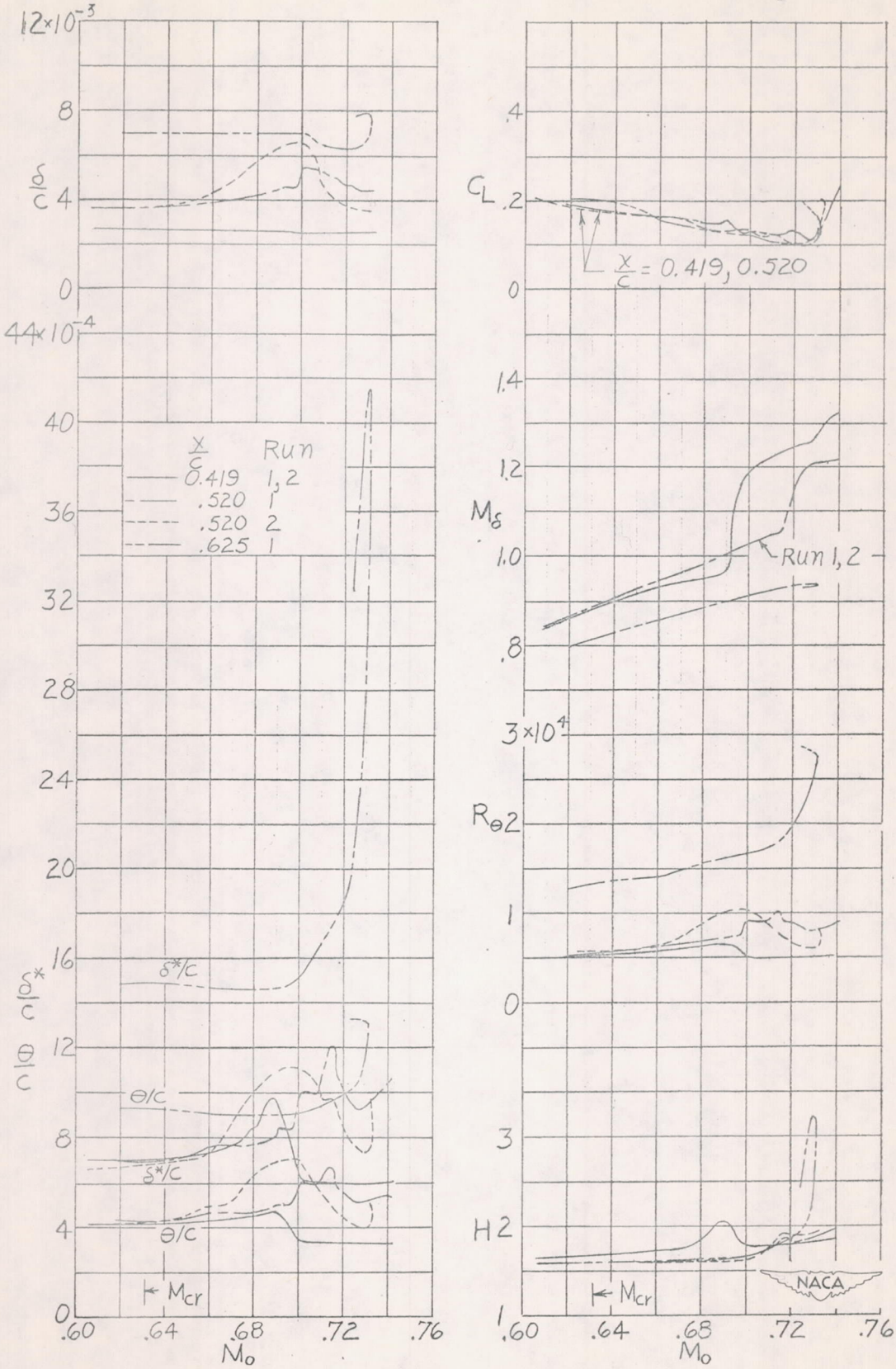

(a) Contour A.

Figure 15.- Variation with M_o of δ^*/c, θ/c, δ/c, H, R_θ, M_δ, and C_L.

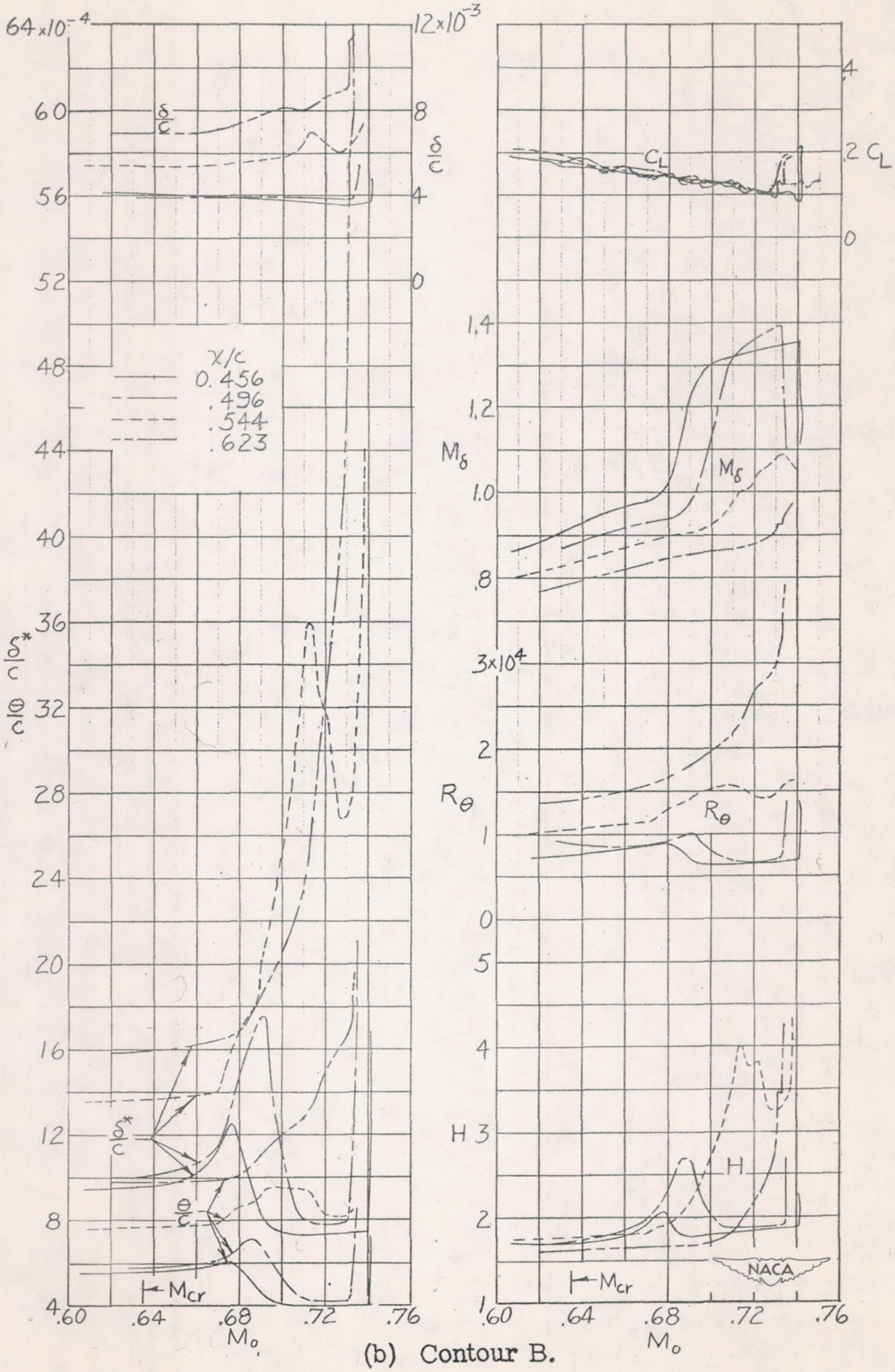

(b) Contour B.

Figure 15.- Conclu

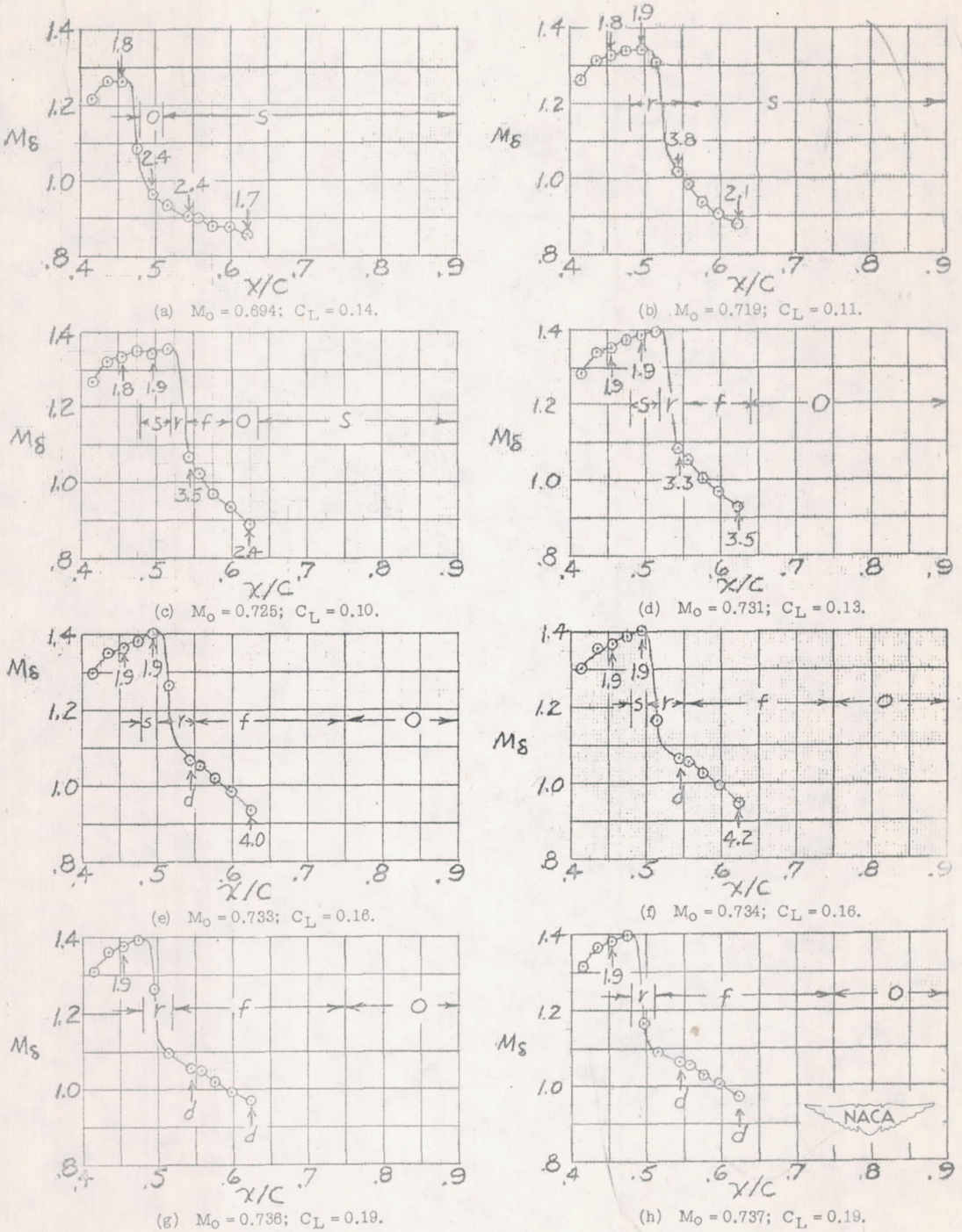

Figure 16.- Correlation of local Mach number distribution, boundary-layer-shape parameter, and surface tuft behavior. Values of shape parameter at various chordwise positions are labeled on M_δ-curves. Symbol "d" indicates flow is advance stages of separation. Tuft behavior is indicated by symbols: "s", tufts undisturbed; "o", tufts oscillating laterally; "r", tufts inclined to surface and oscillating; "f", tufts lying or flipping upstream. Contour B.